Journal of Structural Geology 41 (2012) 47–63

Contents lists available at SciVerse ScienceDirect

Journal of Structural Geology

journal homepage: www.elsevier.com/locate/jsg

Pitfalls among the promises of mechanics-based restoration: Addressing implications of unphysical boundary conditions

Peter Lovely [a,*], Eric Flodin [b], Chris Guzofski [c], Frantz Maerten [d], David D. Pollard [a]

[a] Geological and Environmental Sciences Department, Stanford University, 450 Serra Mall, Stanford, CA 94305, USA
[b] Tengizchevroil LLP, Satpayev Str. 3, Atyrau 060011, Kazakhstan
[c] Chevron Energy Technology Company, 1500 Louisiana St, Houston, TX 77002, USA
[d] Igeoss – A Schlumberger company, Parc Euromédecine, 340 rue Louis Pasteur, 34790 Grabels, France

ARTICLE INFO

Article history:
Received 17 June 2011
Received in revised form
28 February 2012
Accepted 29 February 2012
Available online 20 March 2012

Keywords:
Restoration
Mechanics
Elasticity
Boundary conditions
Normal faults
Volcanic Tableland

ABSTRACT

Mechanics-based restoration has been seen by some in the structural geology community as a panacea – a new technology that melds the retrodeformational merits of kinematic balancing with principles of continuum mechanics. The method has been touted for its ability to simulate complex 3D systems without assumptions of plane strain, allowing for heterogeneous fault slip distributions and mechanical interaction of fault segments. It has been suggested as a means to predict distributions of geologic strain and associated small-scale structures; however, we demonstrate that the kinematics of restoration models may differ significantly from forward deformation. Restoration models are governed by boundary conditions that are different from the forces driving forward geologic deformation. Models may be improved by supplementing restoration boundary conditions with loads that attempt to reverse tectonic strain, but unphysical artifacts persist. Mechanics-based restoration may be an appropriate tool for traditional applications of kinematic models including validation of structural interpretation and modeling geometric evolution; however, more subtle features, particularly strain distribution, should be treated with skepticism. Restoration models may provide insights to the initial configuration of forward mechanical models with physically appropriate boundary conditions and non-linear material behavior. Forward models provide the best means for simulating deformation and predicting subsidiary structures.

1. Introduction

Structural geologists are commonly faced with the challenge of interpreting the present day geometry of complex structures from sparse (e.g. well logs and outcrops) or low resolution and potentially ambiguous (e.g. seismic imaging) data, and with the more daunting task of understanding the evolution of the structure through geologic time from data that is limited to the present. Hence comes a strong appeal for retrodeformational modeling techniques that provide a means to back-step (restore) from the present geometry through the structure's evolution, and a means to evaluate the present state geometric interpretation, by ensuring that the model may be restored to a reasonable initial configuration.

Chamberlain (1910) introduced the concept of the kinematically balanced cross-section in his depth-to-detachment calculation based on conservation of cross-section area and line length of folded strata. New techniques for constructing balanced cross-sections were developed during the 1950's and 1960's (Hunt, 1957; Carey, 1962; Bally et al., 1966), and the concept of the kinematically balanced, fully restorable section was formalized by Dahlstrom (1969).

Dahlstrom's method, designed to model compressional tectonics in the Alberta, Canada foothills, assumes that deformation may be modeled as plane-strain, that cross-sectional area within strata and line length of contacts between strata are conserved throughout deformation, and that all off-fault strain is accommodated entirely by bed-parallel slip. Critical advances in the 1980's (e.g. Boyer and Elliott, 1980; Suppe, 1983) led to a surge in the application of balanced cross-sections and, subsequently, a plethora of ad hoc, empirically derived kinematic mechanisms (e.g. vertical shear (Gibbs, 1983; Williams and Vann, 1987), inclined shear (White et al., 1986; Dula, 1991), and tri-shear (Erslev, 1991; Hardy and Ford, 1997)) have been developed that may mimic nearly any structure in any geologic environment, worldwide. 2D map view (e.g. Rouby et al., 1993) and 3-D kinematic restoration

* Corresponding author. Present address: Chevron Energy Technology Company, 1500 Louisiana St, Houston, TX 77002, USA. Tel.: +1 832 854 6864; fax: +1 832 854 7018.
E-mail address: plovely@chevron.com (P. Lovely).

0191-8141/$ – see front matter © 2012 Elsevier Ltd. All rights reserved.
doi:10.1016/j.jsg.2012.02.020

methods (e.g. Rouby et al., 2000; Griffiths et al., 2002) have been developed that enable structural geologists to move beyond the assumptions of plane-strain and uniform slip on faults. Kinematic methods have become a standard tool for retrodeformational and forward modeling in structural geology, particularly at reservoir and larger scales (e.g. Woodward et al., 1989), and have proven invaluable to structural analysis in the hydrocarbon industry; however, they invoke no causative physical principles and therefore cannot explain how or why a structure evolved as it did (Fletcher and Pollard, 1999; Pollard and Fletcher, 2005).

Additionally, the simplified, ad hoc nature of the kinematic mechanisms governing internal deformation provide strain fields that may not accurately reflect the physical processes that govern rock deformation. For example, kinematic models assume rock is incompressible (conservation of area in cross-section) and therefore cannot accommodate volumetric strain that is pervasive in nature, as evidenced by the abundance of contractional and dilational structures including joints, veins, pressure solution seams, and shear and compaction bands (e.g. Ramsay and Huber, 1983; Pollard and Aydin, 1988; Aydin et al., 2006). As exploration moves to increasingly complicated and hard-to-reach structures, interest in subsurface stress and strain history has increased, with a growing desire to predict small faults, fractures, and other structural features that might influence fluid flow. We seem to have reached the limits of what we may learn from purely kinematic methods.

Forward modeling approaches based on the principles of continuum mechanics overcome these limitations. Mechanical models, commonly implemented numerically in finite element, finite difference, boundary element or distinct element formulations, honor conservation of mass, momentum and energy, and employ a constitutive law to relate stress to strain or rate of deformation. Such methods have been applied to predict displacement, strain, and stress fields associated with reservoir scale fault-related folding (Erickson and Jamison, 1995; Hardy and Finch, 2005; Morgan and McGovern, 2005; Maerten et al., 2006; Benesh et al., 2007; Sanz et al., 2007, 2008; Stockmal et al., 2007), but have the disadvantage that present day geometric observation may not be explicitly incorporated into the model. One must begin with estimates of initial geometric configuration and loading path, and it may be necessary to iteratively adjust in order to obtain a final configuration that resembles a structure as observed in the field.

Mechanics-based restoration methods have been developed by structural geologists over the past decade as a new tool in the arsenal for structural interpretation and evaluation (Muron, 2005; Maerten et al., 2006; Moretti et al., 2006; Plesch et al., 2007; Moretti, 2008; Guzofski et al., 2009). The method, which is described in detail by Maerten and Maerten (2006) and Guzofski et al. (2009), involves generation of a finite element (FEM) volume, composed of discrete tetrahedral elements, which honors the present day observed geometry, followed by restoration, implemented by boundary conditions that flatten one or more deformed stratigraphic horizons to an assumed initial (unfolded and unfaulted) configuration. Those faults explicitly incorporated in the mesh are allowed to slip during restoration such that shear traction is relaxed completely as deformation is propagated through the continuum according to a linear elastic constitutive law. Elasticity, while a great simplification of real rock rheology, lends itself to restoration because its linear nature makes deformation entirely reversible. Schmalholz (2008) demonstrated with viscous folding models that linear viscous (Newtonian) materials exhibit similar retrodeformability. The application of mechanics to restoration represents a novel and necessary innovation in a field traditionally dominated by kinematic methods and seems, on the surface, to be a panacea, coupling the retrodeformational benefits of kinematic models with the physical backbone of continuum mechanics.

Mechanics-based methods offer improvement over traditional kinematic methods by (1) honoring conservation of mass and momentum and employing a constitutive law to derive the kinematic variables, (2) incorporating material heterogeneity in the form of spatially variable elastic moduli, (3) calculating non-uniform slip on faults according to mechanical principles, and (4) accounting for mechanical interaction of fault segments. Particularly for 3D applications in structurally complex regions, the method appears to offer better constrained solutions than kinematic methods. Because these models employ a constitutive law to define a stress–strain relation, theoretical stress fields may be derived from restoration methods. If restoration derived stress, strain, and displacement fields, each of which is mathematically dependent upon the others (Chou and Pagano, 1967), accurately reverse forward deformation, it should be possible to identify regions of intensified stress and strain, as well as principal stress and strain orientations, from mechanics-based restoration models.

To date, it has been assumed that the kinematic properties (strain and displacement) predicted by mechanics-based restoration models are equal in magnitude and opposite in sign to forward deformation. However, despite the mechanical basis of the new restoration methods, unphysical boundary conditions and the limitations of linear elasticity to model rock deformation prove detrimental. We use a series of synthetic and field based examples from the Volcanic Tableland, Bishop, CA, to illustrate the theoretical and practical limitations of boundary conditions applied to mechanics-based restoration models. We suggest several ways to improve linear elastic retrodeformational models, but demonstrate that large, unphysical strain perturbations may be unavoidable when restoration boundary conditions are prescribed, and strain predicted by restoration models should be treated with skepticism. Appropriately sophisticated forward mechanical models, driven by realistic tectonic loading paths, are the best way to predict geologic stress and strain. Mechanics-based restoration, for the reasons described previously, provides improvement over kinematic methods, and should be used to validate structural interpretations and as a guide to infer appropriate initial geometric configuration for forward models. The limitations of elasticity, which may result in stress orders of magnitude greater than the strength of rock, are beyond the scope of this study, but are addressed by Lovely (2011). We therefore address only strain and displacement fields in the remainder of this study.

Before continuing, it is necessary to clarify terminology used throughout the remainder of this manuscript. “Restoration” is used to describe kinematic (displacement) boundary conditions applied directly to the earth’s surface or some deformed horizon, which force that surface to conform to a presumed undeformed state, and to models governed by such boundary conditions. “Reverse” refers to boundary conditions (displacement or traction) that attempt to invert tectonic loading (far-field strain), and are applied to the vertical boundaries of the finite element volume. “Retrodeformation” is used to refer generically to any model (restoration or reverse) that attempts to simulate deformation from the present state to some previous state. A tension positive sign convention is used throughout this manuscript such that extensional strain and corresponding tensile stress have the same sign, and all model results are presented to represent forward deformation.

2. Theory

Linear elastic deformation is perfectly reversible by definition and limited in application to small strain. The principle of superposition, as applied to linear elasticity, states that “two (or more)

stress (or strain or displacement) fields may be superposed to yield the results for combined loads" (Chou and Pagano, 1967, p. 82). Because all of the governing equations are linear, stress, strain and displacement fields are path-independent in linear elastic systems. Therefore, an elastic body deformed by an arbitrary load configuration will return to its initial configuration if those loads are exactly reversed (equal magnitude, opposite orientation). Effectively, this is equivalent to unloading, but it also implies that if one begins with a body geometrically equivalent to the deformed configuration, but free of stress, and applies the reverse load configuration, that body will have the same shape as the original stress-free body, and will be characterized by stress, strain and displacement fields with identical magnitude but opposite orientation to those characterizing the forward deformation. The same might be expected of other linear materials, such as the Newtonian viscous fluid (e.g. Schmalholz, 2008). Any non-linear properties of a mechanical system, including material models (non-linear stress–strain relation) and large deformation (non-linear strain–displacement relation) introduce load path dependency, and therefore forward and retrodeformation will differ.

Additionally, linear elastic deformation, being reversible, does not increase the entropy of a closed system (e.g. Wegner and Haddow, 2009, p. 119). In other words, none of the input work is lost to heat or other irreversible processes such as damage or plastic strain that increase the disorder of the system. Because entropy may not be removed from a closed system, it is assumed that retrodeformation is best performed by a model that results in no additional increase of entropy.

Faults are treated as frictionless in all reverse models because frictionless sliding, like linear elasticity, is reversible. Even the simplest Mohr–Coulomb friction law (e.g. Byerlee, 1978; Jaeger et al., 2007, p. 69) is non-linear and therefore irreversible. The issues relating to friction in reverse models may be understood by considering the stress-state of compressional vs. extensional tectonic settings. While vertical stress is always approximately lithostatic, horizontal compressive stress may be nearly twice as large in a compressional tectonic setting as in an extensional setting (Zoback, 2007). Normal tractions on fault surfaces are greater, and therefore slip is inhibited by friction in a compressional setting. A reverse tectonic model of an extensional system imposes contractional deformation, and the resulting compressive stress across the fault will result in greater frictional strength and reduced slip. The opposite holds true for reverse models of compressional tectonics. While real faults are not actually frictionless, previous studies (e.g. Aydin and Schultz, 1990; Cooke and Marshall, 2006) suggest that the effects of uniform friction do not have a strong influence on mechanical interaction of fault segments, but only on the magnitude of the slip.

Previous authors considering mechanics-based restoration have acknowledged that these models often cannot be used to derive geologic stress, primarily because the elastic constitutive law results in stress magnitudes far greater than those that may be sustained by rock (e.g. Maerten et al., 2006; Guzofski et al., 2009). However, limitations of elasticity aside, restoration models are further plagued by loading that does not exactly reverse the tectonic loads that drove the forward deformation. Unphysical boundary conditions applied to restoration models have considerable implications for both stress-state and kinematics. The fundamental restoration boundary condition consists of vertical displacement imposed on the stratigraphic horizon of interest, which restore it to some presumed undeformed datum (Maerten et al., 2006; Plesch et al., 2007; Moretti, 2008; Guzofski et al., 2009). Displacement boundary conditions imply surface tractions that are mechanically necessary to achieve the displacements.

Orthogonal constraints are necessary at least at one additional point in order to prevent rigid-body translation and rotation, and to define a stable, well-posed boundary value problem. To date, most mechanical restoration efforts have kept additional boundary conditions to a minimum (Maerten and Maerten, 2006; Plesch et al., 2007) or constrained some bounding walls of the FEM mesh to in-plane displacement (Guzofski et al., 2009), while leaving other vertical and horizontal walls of the model as traction-free surfaces. In contrast, forward geologic deformation is driven by tectonic forces in the subsurface, while the earth's surface should be treated as traction-free (e.g. Segall, 2010). Thus, the issues concerning boundary conditions in current mechanics-based restoration methods are two-fold. First, the tractions implied by the restoration boundary condition are a direct violation of the traction-free nature of the earth's surface. Second, treating other surfaces of the finite element model as traction-free fails to reverse the tectonic loading which drove forward geologic deformation.

Mechanics-based restoration models force the kinematic principle of surface restoration, but simulate a different mechanical system from forward deformation. Because the boundary value problem is solved such that the equation of static equilibrium

$$\sum F_i = 0 \tag{1}$$

is satisfied at all points in the volume (e.g. Malvern, 1969; Pollard and Fletcher, 2005), the restoration model, characterized by different surface loads than the true reverse problem, will be characterized by a different stress field throughout the volume. Because stress is related to strain by Hooke's law, resulting strains are not calculated correctly, and because strain is the derivative of displacement, calculated displacement is correspondingly erroneous.

3. Synthetic example

The reversible nature of elasticity given precise reversal of forward loads and the qualitative implications of unphysical restoration boundary conditions are illustrated by a 2D synthetic example with a single normal fault (Figs. 1 and 2) in a homogeneous elastic body. Deformation is driven by 10% horizontal extension. The model base is fixed vertically and the upper surface is traction-free. The fault surface is allowed to slip without frictional resistance, but separation and interpenetration are prohibited. It is important to note that here, and throughout this manuscript, strain from retrodeformational models is calculated in a forward deformational sense. The mesh is retrodeformed according to the calculated displacement vectors and then the sign of displacement vectors is changed to reflect forward deformation prior to calculating displacement gradient and strain components.

Magnitude and orientation of maximum principal strain calculated from forward and reverse models are presented in Fig. 1a and b, respectively. As predicted by the linear elastic principle of superposition, deformation fields predicted by forward and reverse elastic models are very similar, although not identical due to numerical imprecision and non-linear geometric effects. The red dashed line in Fig. 1b represents the outline of the original forward model, prior to deformation. The deformed geometry, subjected to reverse boundary conditions, matches the initial undeformed geometry almost perfectly.

In contrast to the similarity between strain distributions calculated from forward and reverse models, strain distributions calculated from restoration models (Fig. 1c and d) differ significantly. We present two different restoration models, one in which vertical displacement constraints are imposed on the model base (Fig. 1c), as in the forward model, and one in which the base is treated as a free surface (Fig. 1d). In the case of these synthetic examples, we

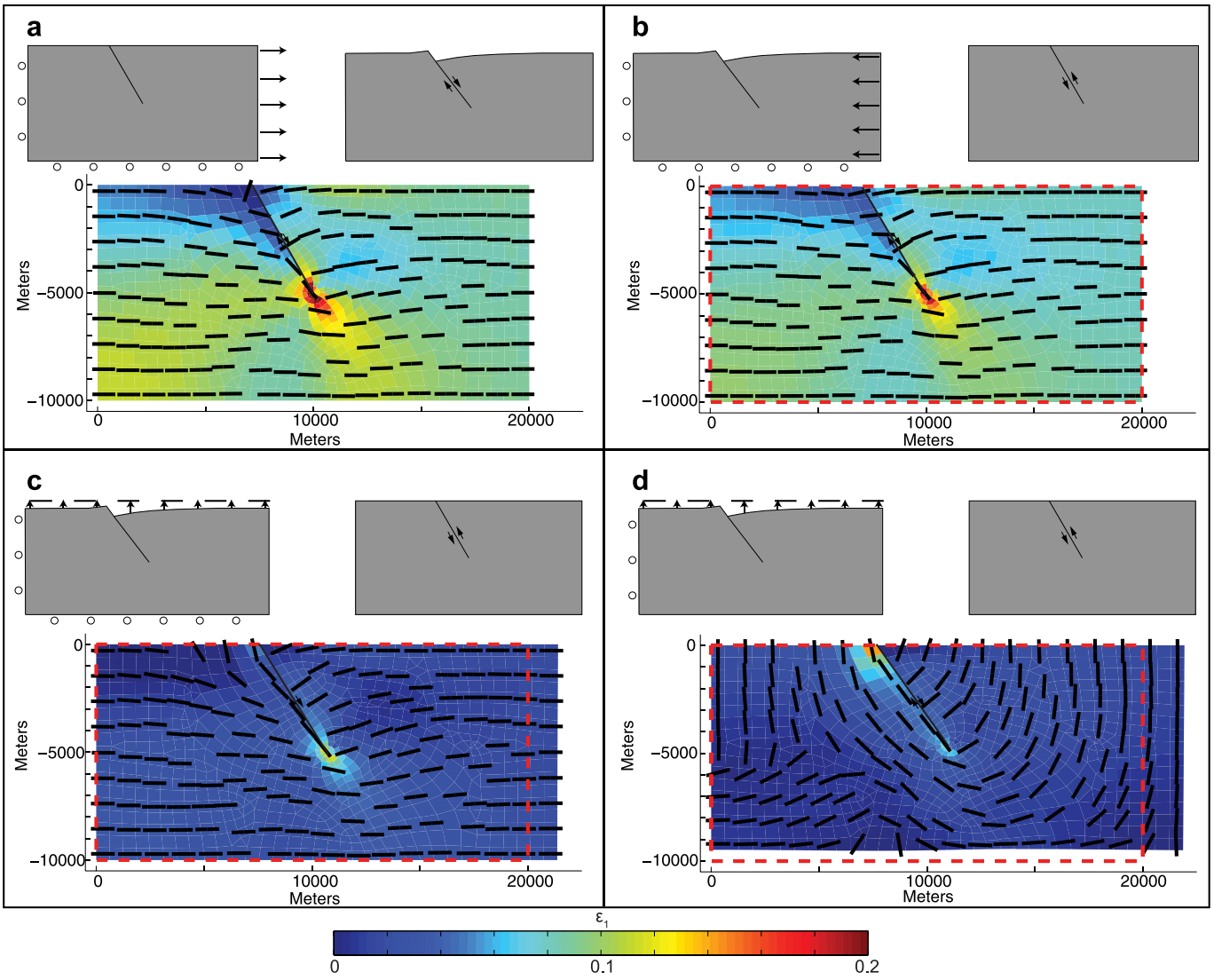

Fig. 1. Model configuration and results representing slip on an idealized frictionless normal fault in a two-dimensional elastic body for a) forward model, b) reverse model, c) restoration model with vertically constrained base, and d) restoration model with unconstrained base. Top: schematic illustrations of the initial model configuration and boundary conditions (left) and the deformed model configuration (right). The initial geometric configuration of retrodeformational models (b, c & d) is equivalent to the deformed configuration of the forward model (a). Bottom: Maximum principal strain magnitude (color contours) and orientation (black vectors) calculated for forward deformation. The red dashed box in b, c & d represents the outline of the undeformed forward model.

are fortunate to know the initial thickness of the undeformed model exactly, which enables us to impose constraints on the model base that accurately restore the initial thickness. When dealing with real geologic data, the undeformed thickness of a single stratigraphic unit or package of units is probably difficult to constrain. For this reason, published examples of mechanics-based restoration (e.g. Maerten et al., 2006; Plesch et al., 2007; Guzofski et al., 2009) have treated the model base as a traction-free surface. Field examples investigated later in this study do the same. Although neither restoration model accurately represents the strain distributions associated with forward deformation, imposing thickness constraint (Fig. 1c) does improve principal strain orientations. In the restoration model with a free base (Fig. 1d), neither orientation nor magnitude of model strain represents forward deformation; however, when the base is constrained to enforce appropriate thickness in the restored model (Fig. 1c), maximum principal strain is generally sub-horizontal, in agreement with the forward model.

As in Fig. 1b, the red dashed lines in Fig. 1c and d represents the outline of the initial model, prior to forward deformation. Both models driven by restoration boundary conditions restore to geometric configurations that differ markedly from the initial geometry of the forward model. Specifically, the horizontal dimension of each restoration model exceeds the horizontal dimension of the initial geometry by nearly 2 km (10%), the magnitude of extension applied to the forward model. Additionally, the thickness of the restored geometry in the model with the unconstrained base is several hundred meters less than the initial geometry. In restoration models, the horizontal component of the strain tensor and, correspondingly, the displacement of the free vertical boundary do not reflect the forward model because the restoration model fails to capture the horizontal tectonic extension that drove fault slip during forward deformation. This failure is a direct result of treating vertical model boundaries as traction-free surfaces.

Potentially detrimental kinematic limitations of restoration boundary conditions (BCs) are further emphasized by examination of slip distributions resulting from the same forward and retrodeformational models, representing a single normal fault in an elastic half-space (Fig. 2a). The forward model generates a semi-elliptical slip distribution, which is reproduced almost perfectly

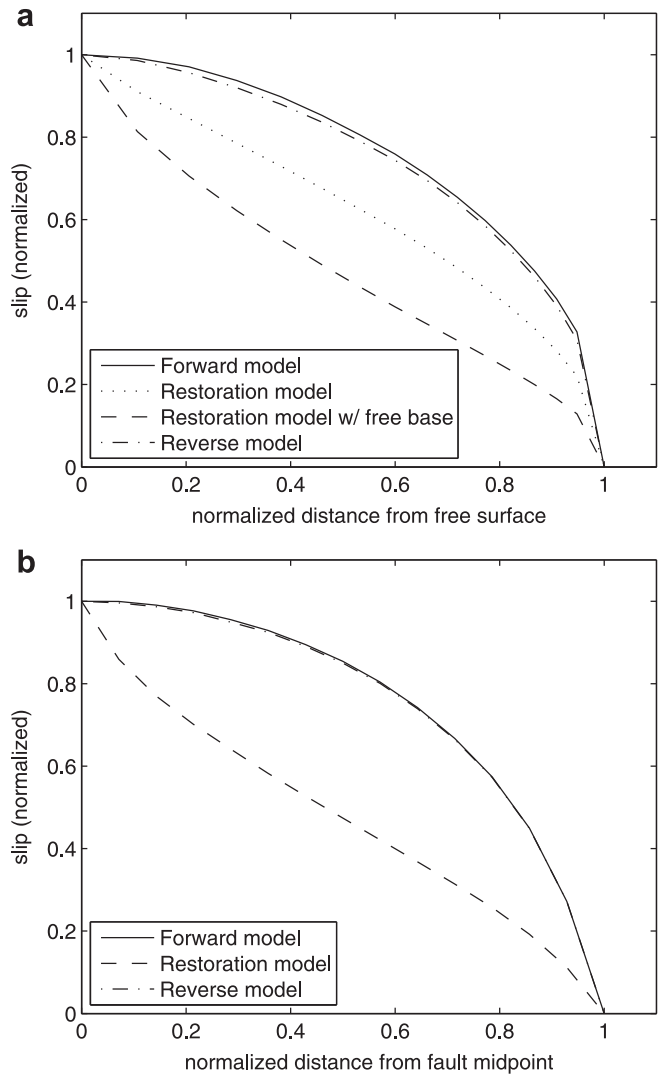

Fig. 2. Normalized slip distribution for forward and retrodeformational models of an idealized fault in a homogeneous elastic body. a) The same four models presented in Fig. 1, representing a normal fault that intersects the model's traction-free surface. b) Models representing a normal fault that is distant from any other boundaries.

by the reverse model; however, models governed by restoration BCs generate slip distributions that are characterized by steep slip gradients at both ends of the fault, approaching the earth's free surface, as well as the fault tip at depth, with a lesser slip gradient in between. Slip magnitude is under-represented everywhere between the endpoints. We note that the restoration model in which the model base is constrained to zero vertical displacement, as it is in the forward model, generates a slip distribution that resembles the forward model substantially better than the restoration model in which the model base is treated as traction-free. Although geologic deformation is not purely elastic in nature, and therefore geologic slip distributions may not exhibit the ideal semi-elliptical shape (e.g. Burgmann et al., 1994; Willemse et al., 1996; Kattenhorn and Pollard, 2001; Manighetti et al., 2001), the idealized elastic example highlights the potentially detrimental implications of boundary conditions on the kinematics of mechanics-based restoration models. Such effects must be considered when interpreting restoration model results.

A potential criticism of the analysis presented above, and of the following field based example, is that the scenarios represent worst-case, end-member examples because the restoration boundary condition prescribes displacement, and therefore results in traction, on a surface that should be traction-free. In many situations, restoration BCs are naturally prescribed to the earth's free surface, for example if one is interested in sequential restoration of growth strata to their assumed geometry when they were deposited on the earth's surface (e.g. Guzofski et al., 2009). However, restoration of a deeply buried surface merits consideration. Perhaps the implications of the restoration BC would be less detrimental if they were prescribed to a surface that is not naturally traction-free.

We consider a model with a single fault that dips 45° and is several fault-lengths distant from each model boundary. By subjecting the model to uniaxial, horizontal, tensile stress, we effectively simulate the behavior of an infinitely long, frictionless normal fault in an elastic whole space. The reverse model considers the deformed geometry subjected to uniaxial horizontal compression, and the restoration model flattens an originally horizontal line that passes through the fault's mid-point by prescribing vertical displacements. Forward and reverse models generate elliptical slip distributions that are very similar to each other, but the restoration model generates a slip distribution that under-represents the forward model (Fig. 2b). The restoration model exhibits a steep slip gradient at the fault's intersection with the restored surface. The slip distribution over the fault's half-length, from mid-point to tip, as calculated from the whole space restoration model, is very similar to the slip distribution calculated from the restoration model in which BCs are prescribed on the earth's free surface. Results suggest that the potentially detrimental effects of restoration BCs are not exaggerated in the end-member case in which the restored surface represents the earth's traction-free surface. Therefore, the implications of this study, which focus on restoration of the free surface, should apply to most mechanical restoration models, even if the restored surface does not correspond to the earth's traction-free surface.

It is worth noting that only by considering an example in which the restored surface coincides with the fault's mid-point, and the point of maximum slip, are maximum slip in forward, reverse and restoration models identical. If the restored surface does not intersect the fault at its mid-point (or at the point of maximum slip if it does not coincide with the mid-point), restoration model slip, which already under-represents forward deformation, as described above, would likely be even less.

Strain distributions for the whole space model are not presented, but the effect of the restoration boundary condition is to generate a strain concentration in the vicinity of the intersection of the fault and restoration surface, similar to the strain concentration at the intersection of the fault and the free surface in the examples presented previously (Fig. 1c and d). This strain concentration is absent from forward or reverse models, and there is no apparent reason to suggest it might have geological significance.

If the restoration BC were prescribed on a surface that does not intersect the fault, the local, unphysical strain that has been observed at the intersection point would not develop. We have not explicitly considered this situation; however, the restoration BC remains unphysical and other detrimental effects would undoubtedly persist. Additionally, as in models in which the earth's free surface is restored, the whole space restoration model fails to account for the strain resulting from the far-field stress that drives slip in forward models.

4. Analysis of field data

In the following section, we consider the challenges of retrodeformational modeling in the context of 3D field data from the extensional fault system of the Volcanic Tableland, Bishop, CA. The

approach parallels that presented previously for synthetic models; however, we address the complications of retrodeformational modeling that arise due to imperfect models and real geologic data. While the synthetic model could be retrodeformed almost perfectly by reversing the boundary conditions of the forward model, two new challenges arise when dealing with a real geologic system. First, appropriate reverse boundary conditions are usually poorly constrained. In most geologic applications, strain history is not well known. Poor constraint on regional geologic strain is a primary reason why previous mechanics-based restoration efforts have treated vertical bounding surfaces as traction-free – it has been considered best to omit constraint entirely where accurate constraint is unavailable. We advocate using a mechanics-based paleostress analysis to help overcome this limitation, but acknowledge that this technique may be inadequate in some cases.

Second, even with optimized far-field loads, reverse boundary conditions fall short of restoring the horizon of interest to its assumed undeformed state. More complicated and potentially heterogeneous far-field BCs, inelastic continuum deformation, and deformation associated with geometric complexities of structures beyond model resolution and structures omitted from the model for simplicity are just a few of the numerous limitations that may prevent a reverse elastic model from adequately flattening a faulted and folded horizon. Thus, we consider models that couple reverse tectonic loads and restoration boundary conditions, and demonstrate that such models offer significant improvement over traditional mechanics-based restoration, but that they continue to suffer from the shortcomings of unphysical restoration boundary conditions. Ultimately, we conclude that forward mechanical models are the best path forward to simulate geological stress, strain and displacement, but we suggest that pure reverse elastic models or mechanics-based restoration models supplemented by reverse tectonic boundary conditions may help to develop a more appropriate forward model, and to understand the limitations thereof.

4.1. Geological setting

The Volcanic Tableland, north of Bishop, CA, in the Owens River Valley, boasts one of the world's premier field exposures of a young, evolving extensional fault system. Pinter (1995) mapped the fault system in great detail, and the site has become a classical field laboratory for studies investigating normal fault slip distributions and growth (Dawers et al., 1993; Dawers and Anders, 1995; Willemse et al., 1996; Ferrill et al., 1999). It has also been the field site of studies investigating fault kinematics (Ferrill et al., 2000; Ferrill and Morris, 2001), micro-scale deformation mechanisms (Evans and Bradbury, 2004) and fault zone permeability (Dinwiddie et al., 2006). The Volcanic Tableland is a plateau, formed by the weathering resistant surface of the Bishop Tuff, a welded ash flow that erupted 757,000 +/− 9000 years ago (Izett and Obradovich, 1994), from the Long Valley Caldera, roughly 40 km to the northwest (Bailey et al., 1976). The tuff consists of a thin (7–8 m), densely welded unit that caps the sequence and defines the topography, with deeper layers that are characterized by lesser degrees of welding, to reach a total thickness of 70–150 m in the study area (Wilson and Hildreth, 1997; Evans and Bradbury, 2004). The tuff is underlain by 1–2 km of volcanic, alluvial and lacustrine sediments, themselves underlain by crystalline basement (Hollett et al., 1991). Gilbert (1938) and Bateman et al. (1965) present a comprehensive overview of the Tableland and surrounding geology.

The Tableland fault system consists of over 100 distinct scarps, of which trace lengths sum to several hundred kilometers. Most of the faults strike roughly north–south. Some dip to the east, and others west. Scarps range from tens of meters to greater than 10 km in length, and maximum throw ranges from less than 1 m to about 150 m. The Fish Slough fault (FSF), on the eastern edge of the Tableland, stands out among the faults, as it is about three times larger than any other fault as measured by length or maximum throw.

The Owens River Valley is located at the western edge of the Basin and Range province, and at the northern end of the Eastern California Shear Zone. The large basin-bounding faults, including the White Mountain fault to the east of the Tableland (Fig. 3, inset), accommodate kilometers of extension and right-lateral strike-slip (Stockli et al., 2003; Kirby et al., 2006). Geologic and geophysical evidence suggests, however, that Tableland extension is primarily east-west, and the faults accommodate primarily dip-slip (Bateman et al., 1965; Dawers et al., 1993; Dawers and Anders, 1995).

The Volcanic Tableland is an ideal site for a 3D field based study of fault mechanics using linear elastic theory because infinitesimal strain may be a realistic approximation. Lovely (2011) demonstrate that, despite relatively small strain, inelastic deformation is prevalent, but that simplified elastic models capture the kinematics relatively well. Fault scarp geometries and slip distributions suggest substantial mechanical interaction between nearby faults (Dawers et al., 1993; Dawers and Anders, 1995; Willemse et al., 1996), behavior that cannot be modeled in 2D or by kinematic methods. The weathering resistant surface of the tuff represents a time-stratigraphic marker (Ferrill et al., 1999) and comparable recent tuff ash flow deposits such as that deposited in the Valley of Ten Thousand Smokes during the 1912 eruption of Katmai Volcano, Alaska (Griggs, 1922) suggest that the top of the Bishop tuff may be approximated as planar at the time of deposition. Erosion and deposition are thought to be less than 1–2 m across the Tableland (Goethals et al., 2009), much less than fault-related topography (10's of meters, up to 150 m). Thus, surface topography and small faults may be resolved more precisely than in subsurface seismic imaging data, and kinematically appropriate restoration boundary conditions may be defined with ease.

4.2. Geological model

Three-dimensional numerical models of fault-related deformational systems require 3D surface representations of fault geometry. Unfortunately, subsurface data is not available at the Tableland, so we use a coarse optimization procedure to infer fault geometry from topography and fault traces extrapolated to depth. 96 trial fault geometries with variable dip and depth of faulting were implemented in a linear elastic half-space in the boundary element code Poly3D (Thomas, 1993; Maerten et al., 2009), and subjected to uniaxial east-west (fault-perpendicular) extension. Strain magnitude was optimized independently for each trial fault geometry, following which the optimal geometric configuration was selected as that which minimized the difference between topography and vertical displacement of the model earth surface. Results suggest that fault dip is relatively shallow, approximately 50°, and faults extend to about 750 m depth. The depth of Fish Slough fault was treated independently due to its greater length and throw, and its inferred depth is 2000 m. Details of the modeling process are described by Lovely (2011).

The fault model used for numerical simulations in this study represents only seismic-scale faults – that is, faults that would likely be easily discernible in typical industry quality seismic imaging data. Those faults with consistently greater than 20 m throw are identified in an unbiased manner by a simple algorithm that scans the DEM for topographic features that are sufficiently large and continuous. Fourteen seismic-scale faults were identified, including two distinct segments of the Fish Slough fault, and are implemented as sliding contact surfaces in models. Seismic-scale

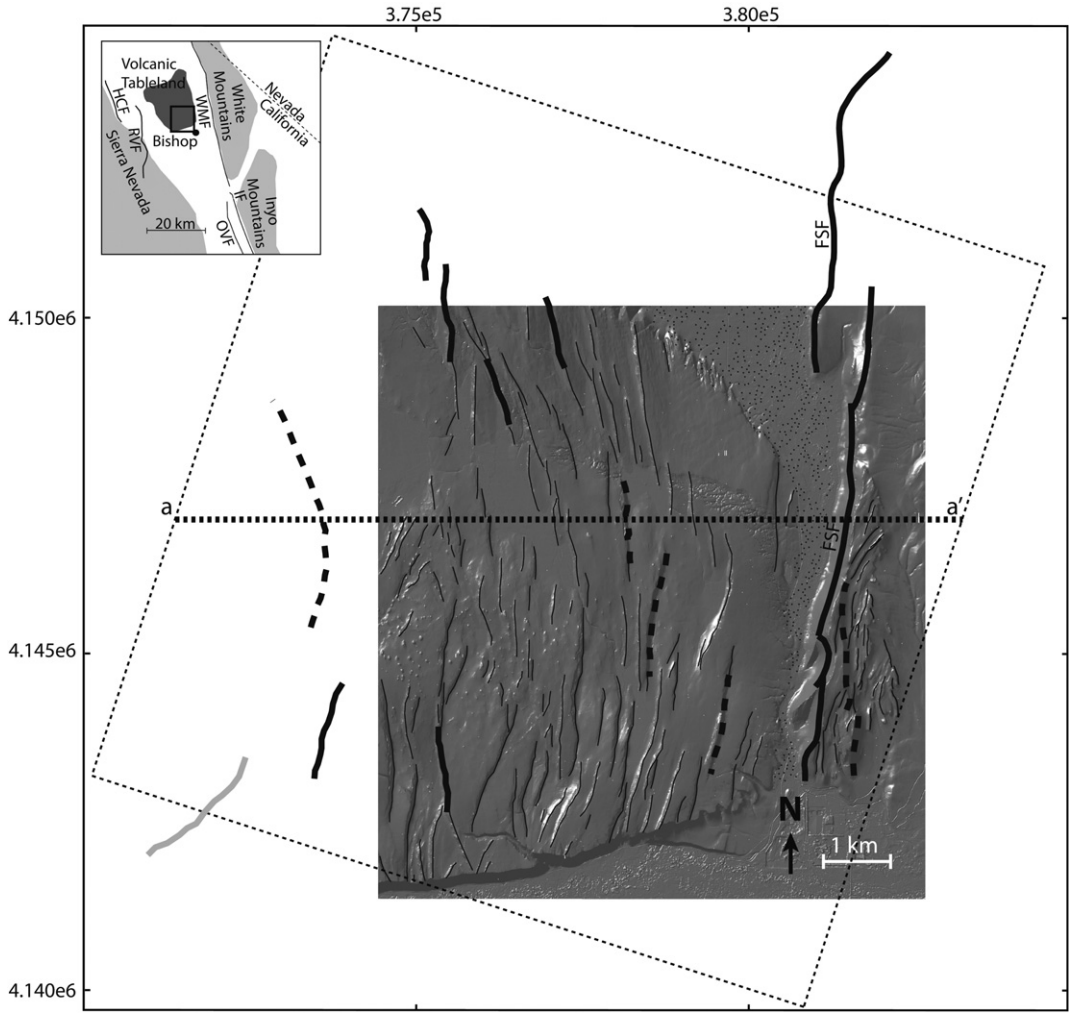

Fig. 3. Map of the Volcanic Tableland study area. Hillshade image represents topography from 2 m (6.6 ft) DEM acquired by ALSM. Thin lines represent fault scarps identifiable from ALSM data. Bold solid lines represent west-dipping seismic-scale faults and bold dashed lines represent east-dipping seismic-scale faults. The bold grey line in the southwest corner represents a fault slightly below the seismic-scale threshold, which is used only for paleostress analysis. The dotted line represents the extent of the FEM mesh used for DynelI3D models and the bold dotted line a–a' represents the location of cross-sections presented in Figs. 5–7. Stippled region represents the extent of alluvium in Fish slough, where the upper surface of the Bishop tuff has been eroded and fault scarps may be obscured. Inset: regional map of Tableland vicinity. Abbreviations: WMF – White Mountain fault; HCF – Hilton Creek fault; RVF – Round Valley fault; IF – Inyo fault; OVF – Owens Valley fault; FSF – Fish Slough Fault.

faults are identified by bold lines in Fig. 3. This limited fault selection (as opposed to including all of the hundreds of faults discernible in the DEM or in the field) minimizes numerical instabilities, maintains a computationally feasible problem, and reduces complications inherent to 3D finite element mesh generation. This selection of faults offers the additional benefit of providing a direct analog to the fault model that might be generated from interpretation of seismic reflection data, but the outcrop exposure provides an opportunity to map smaller structures for comparison with restoration strain distribution, as well.

All numerical models of the Tableland, forward and retrodeformational, are implemented in a homogeneous elastic medium. The homogeneous elastic model is a significant simplification of the complicated local geology. However, stratigraphy beneath the tuff is not well known and the depth of sediments overlying crystalline basement rocks is poorly constrained, so lithologic heterogeneities cannot be accurately defined. The Bishop Tuff and underlying units do not deform as a perfectly elastic material, as evidenced in the field by abundant fractures and by the unrealistic tensile stress magnitudes suggested by the paleostress analysis (Appendix A). However, linear elasticity is necessary for mechanics-based retrodeformational models and inelastic behavior is not the focus of this study. We elect to implement a homogeneous material model for several reasons. The stratigraphic heterogeneity of the tuff is well below the resolution of the finite element mesh, and therefore cannot be accommodated, and other subsurface heterogeneities are poorly constrained.

Elastic moduli are selected from laboratory tests investigating properties of tuff found at Yucca Mountain, Nevada, which have a similar composition to the Bishop Tuff. Laboratory measurements are scaled to account for the damage inherent to large rock masses and observed (e.g. fractures) in the Bishop Tuff. Laboratory measurements suggest Young's moduli ranging from 2 to 33 GPa, depending on the degree of welding and porosity (Lin et al., 1993; Avar et al., 2003). Although the uppermost welded layer would undoubtedly be quite stiff at the scale of a laboratory sample, the densely welded unit is thin (7–8 m) and highly fractured. We use a Young's modulus of 2.5 GPa, considering that most of the tuff is only slightly welded and that the effective stiffness of rock at outcrop and larger scales is approximately 20–60% that of a laboratory sample (Bieniawski, 1984). Poisson's ratio for numerical models is selected as 0.25 (Lin et al., 1993).

4.3. Paleostress analysis to determine reverse tectonic boundary conditions

Unlike the ideal synthetic example, in which geometric configuration is known precisely and forward deformation is perfectly linear, and thus perfectly retrodeformed by reverse boundary conditions, reverse tectonic boundary conditions must be estimated for a real geologic setting. Paleostress analysis provides a means to define far-field boundary conditions for elastic models that accurately reproduce fault slip distributions observed in the field. In many geologic settings, total regional strain throughout the deformational history is poorly known. Restorations are, in fact, commonly used to estimate tectonic extension or contraction (e.g. Allmendinger et al., 1990), despite the fact that the kinematic methods generally employed account only for strain accommodated by fault slip and assume that no extension is accommodated by continuum rock deformation. We suggest using a mechanics-based paleostress analysis to determine far-field loads for elastic models, though we acknowledge that such analysis may be difficult or impossible to perform in the cases of some particularly complex or highly deformed structures. In such situations, however, even a coarse estimate of regional loading, such as kinematic estimates of extension/contraction or traction BCs estimating in-situ stress, should provide a more sound retrodeformational model than one in which vertical boundaries are treated as traction-free. The Volcanic Tableland, with abundant faults spanning a broad range of size, all of which may have been active simultaneously during the Tableland's geologically brief history, is an ideal setting to implement paleostress analysis. Detailed methods and results of paleostress analysis using mechanics, as applied to the Volcanic Tableland, are described in Appendix A.

4.4. Numerical models

Retrodeformational models of the Volcanic Tableland are peformed using Dynel3D©, a commercially available finite element (FEM) package from IGEOSS (http://www.igeoss.com), which has been developed with mechanics-based restoration in mind. Forward models are performed using Poly3D, which is based on a boundary element formulation. The FEM lends itself to retrodeformational modeling because models may accommodate geometric complexities such as faulted and folded stratigraphic horizons, and particularly to restoration boundary conditions because displacement may be prescribed at nodes on the boundaries of, or within, the elastic continuum. However, finite element models require that the entire volume be discretized by 3D tetrahedral or hexahedral elements, which poses challenges for mesh generation and leads to computationally cumbersome solutions as the number of elements grows rapidly. As a result, relatively coarse mesh discretization is necessary to maintain a computationally feasible solution. Boundary elements are computationally advantageous because only fault surfaces need to be discretized as triangular elements of displacement discontinuity in 3D space; however, initial model geometry must be simple, either a whole- or half-space in Poly3D, and boundary conditions may be prescribed only on the faults as either displacement discontinuity (slip or opening) or traction. It is difficult to incorporate complicated 3D surface topography or to prescribe restoration boundary conditions in the half-space boundary element model.

The FEM mesh representing the Volcanic Tableland, which is used for all Dynel3D retrodeformational models, includes the seismic-scale fault model introduced previously (each fault is represented by frictionless sliding contact surfaces) and the upper surface of the volume conforms to topography as defined by the National Elevation Dataset 1/3 arc-second (~10 m) DEM. ALSM coverage is not sufficient to define the entire extent of the restoration model (Fig. 3), and because mesh resolution is only 250 m, the 10 m DEM is sufficient for this application. Mean relative error of the DEM at a kilometer scale is 1.64 m, with a standard deviation of 2.08 m (Maune, 2007), which is significantly better than precision of seismic reflection images (Yilmaz and Doherty, 2001).

As discussed in the following section, it is essential that the finite element mesh have a rectangular shape in map view, with edges perpendicular to far-field principal stress trajectories, in order to define simple and appropriate reverse tectonic boundary conditions. Therefore, it was necessary to extrapolate topography south of the Tableland where the Bishop Tuff has been eroded. Similarly, it was necessary to extrapolate the surface of the tuff from west-to-east across Fish Slough and into the footwall of the Fish Slough fault, because the welded tuff has been eroded or is covered by alluvium in the slough. Analysis focuses on an east–west cross-section a–a' through the 3D model at 4,147,000 m northing (Fig. 3), in a region where the implications of extrapolating topography should be minimal. The mesh, shown in Fig. 4, covers an area of roughly 11 × 11 km (Fig. 3), extends to 4 km depth, and consists of 339,816 tetrahedral elements. In contrast, the Poly3D forward models consist of only 3603 triangular elements, and resolution is improved, with each element roughly 180 m on a side.

Four different models of the Tableland are considered, representing (1) forward deformation, (2) restoration boundary conditions only, (3) restoration boundary conditions supplemented by optimized (paleostress) reverse tectonic boundary conditions, and (4) optimized, though imperfect, reverse tectonic boundary conditions alone. Forward models performed using Poly3D may be governed by far-field boundary conditions directly from paleostress analysis. In the model with restoration boundary conditions only, vertical displacement is prescribed such that topography is flattened to $Z = 0$ and all other boundaries of the FEM mesh are treated as traction-free.

Restoration boundary conditions may be supplemented by additional constraints that reverse the tectonic loading that drove forward deformation. In finite element models, it is impossible to prescribe true far-field stress or strain boundary conditions, and the

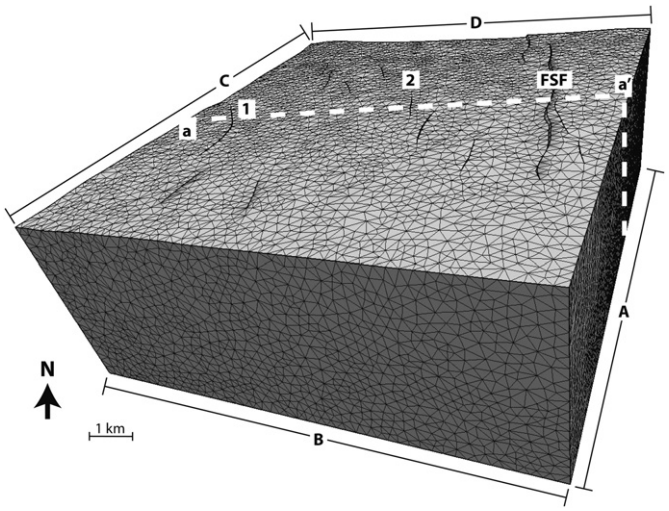

Fig. 4. Undeformed FEM mesh representing the Volcanic Tableland system in its present state. The white dashed line a–a' represents the location of cross-sections presented in Figs. 5–7. Faults labeled "1", "2", and "FSF" are correspondingly labeled on cross-sections.

Dynel3D interface does not accommodate traction boundary conditions. Thus, it is necessary to simulate reverse tectonic boundary conditions by prescribing on vertical model boundaries displacements that best reproduce far-field paleostress conditions. This is most easily done by defining a model volume (Fig. 3) that is rectangular in map view with vertical edges perpendicular to horizontal principal stress trajectories. Face-perpendicular displacement is prescribed on the four vertical model boundaries (A, B, C & D as identified in Fig. 4), but nodes on these boundaries are free to displace within the plane of the boundary such that the surface is shear traction-free. Face-perpendicular displacement on boundaries A & B is zero and appropriate displacements are calculated for boundaries C & D such that the net strain of the volume is equivalent to far-field strain derived from paleostress analysis. Reverse boundary conditions for the Tableland model consist of displacing boundary C 229 m toward boundary A, and boundary D 162 m toward boundary B.

ε_{zz} is never imposed, but rather either the upper or lower model boundary is always treated as traction-free. The model base is treated as traction-free in both restoration models because there is no way to provide improved constraint without prior knowledge of the initial (undeformed) thickness of those units represented by the model. The reverse model is governed by the same reverse tectonic boundary conditions as described above, but unlike the previously described model in which restoration boundary conditions are applied to the earth's surface, the earth's surface is traction-free and zero vertical displacement is prescribed on the model base. Such vertical boundary conditions result in zero average vertical stress, which is appropriate for a model that does not account for lithostatic load, though vertical stress may be locally large near where displacements are prescribed (hence the issues with restoration boundary conditions).

4.5. Results

Discussion of mechanics-based retrodeformational models of the Volcanic Tableland focuses on plots of maximum principal strain (Fig. 5), vertical strain (Fig. 6) and displacement vector fields (Fig. 7) from the four models described previously. Each retrodeformational model (restoration BCs only, restoration BCs supplemented by reverse tectonic BCs, and reverse tectonic BCs only) are compared to the forward model to evaluate the limitations. A comparison of results of the four Tableland models (forward and retrodeformational) is presented in Table 1.

Patterns of all kinematic variables investigated differ markedly between forward models and retrodeformational models with only restoration BCs. Retrodeformational models with restoration and reverse tectonic BCs generally exhibit kinematics more similar to forward models and retrodeformational models with reverse BCs only are most similar to forward models. Unlike the idealized synthetic models discussed previously, forward models and retrodeformational models with reverse tectonic BCs are not identical; however, the largest differences may be attributed to the numerical methods (BEM for forward models and FEM for retrodeformational models). For example, the rotation of ε_1 evident in the footwall of FSF in the retrodeformational model with reverse BCs only (Fig. 5d) is likely an artifact of the nearby model boundary; quadrants of extension and contraction at fault tips in the reverse tectonic model are poorly defined due to the coarse discretization of the finite element mesh.

5. Discussion

Comparison of forward and retrodeformational models presented in Figs. 5–7 and Table 1 highlights the importance of carefully considering the implications of boundary conditions in mechanics-based restoration models. We select the forward elastic model as a basis for comparison and evaluation of models with restoration boundary conditions not because the forward model is necessarily the best available representation of Volcanic Tableland deformation (the elastic constitutive law and seismic-scale fault model, among other features, make this a highly simplified model), but because it honors principles of continuum mechanics, including conservation of mass, momentum and energy, the kinematic variables are derived through implementation of an established, though simplified, constitutive law relating stress and strain, and deformation is driven by boundary conditions that resemble tectonic strain in orientation, distribution, and magnitude. We do not consider a more appropriate inelastic constitutive law for forward models in order to maintain our focus on evaluating the implications of boundary conditions and to enable a direct comparison with elastic retrodeformational models.

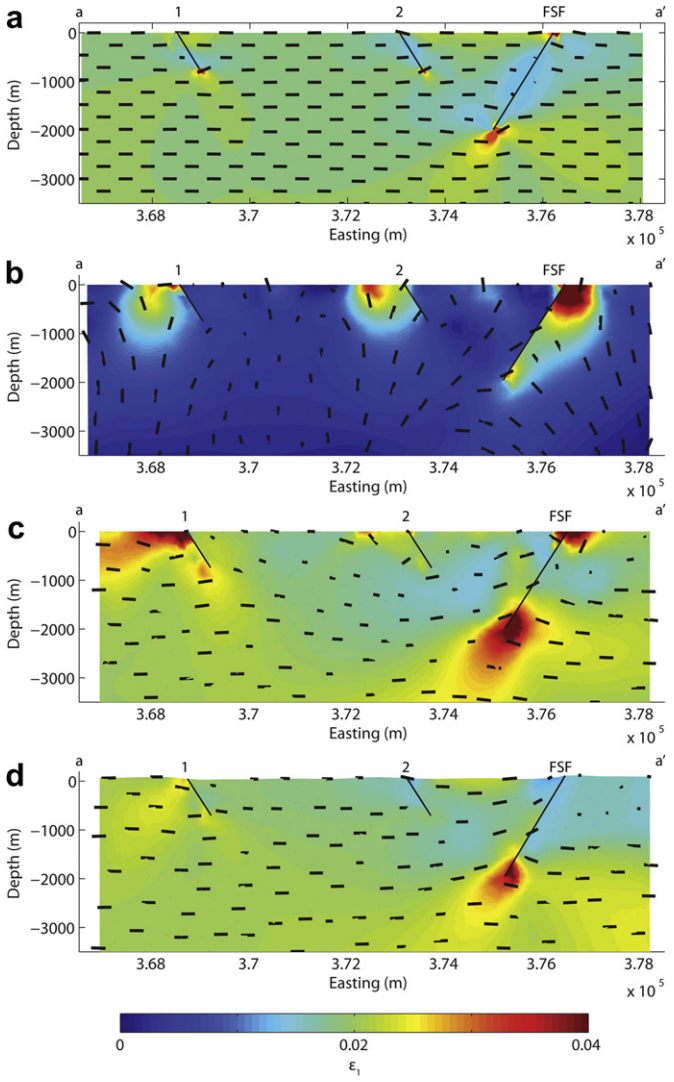

Fig. 5. Maximum principal strain magnitude and orientation on cross-section a–a' (Fig. 3) as calculated by a) forward model in Poly3D, b) restoration boundary conditions alone, c) restoration boundary conditions supplemented by reverse tectonic boundary conditions, and d) reverse tectonic boundary conditions alone. Note that principal strain orientation vectors are plotted in 3D. Thus, short vectors indicate that a large component of ε_1 is out of the plane of the cross-section, and long vectors indicate that ε_1 is almost entirely in the cross-section plane.

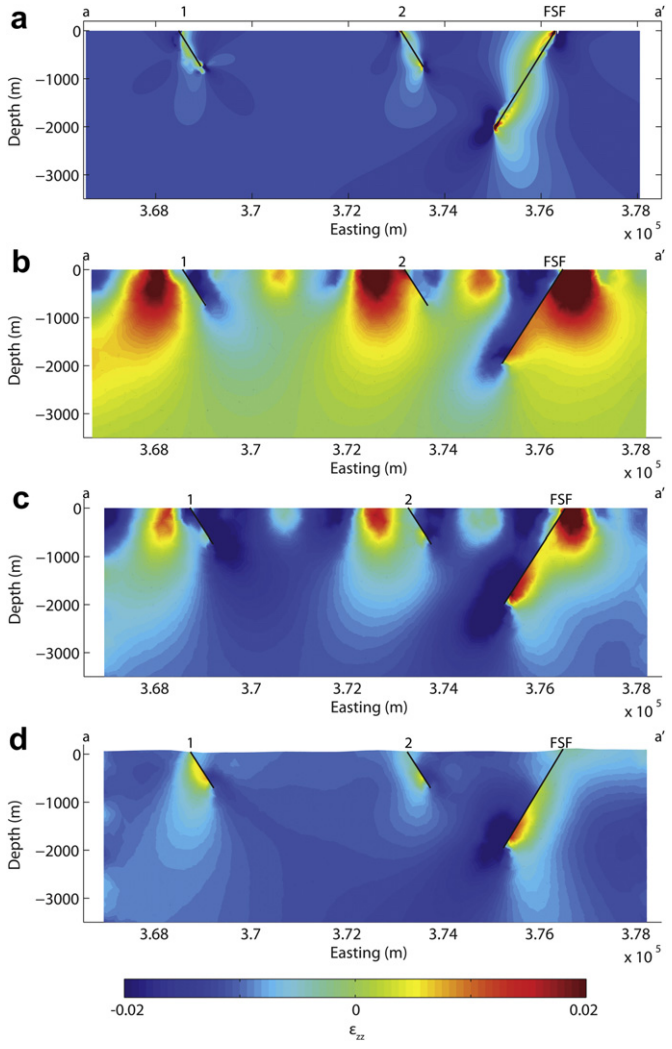

Fig. 6. Vertical strain magnitude on cross-section a–a' (Fig. 3) as calculated by a) forward model in Poly3D, b) restoration boundary conditions alone, c) restoration boundary conditions supplemented by reverse tectonic boundary conditions, and d) reverse tectonic boundary conditions alone.

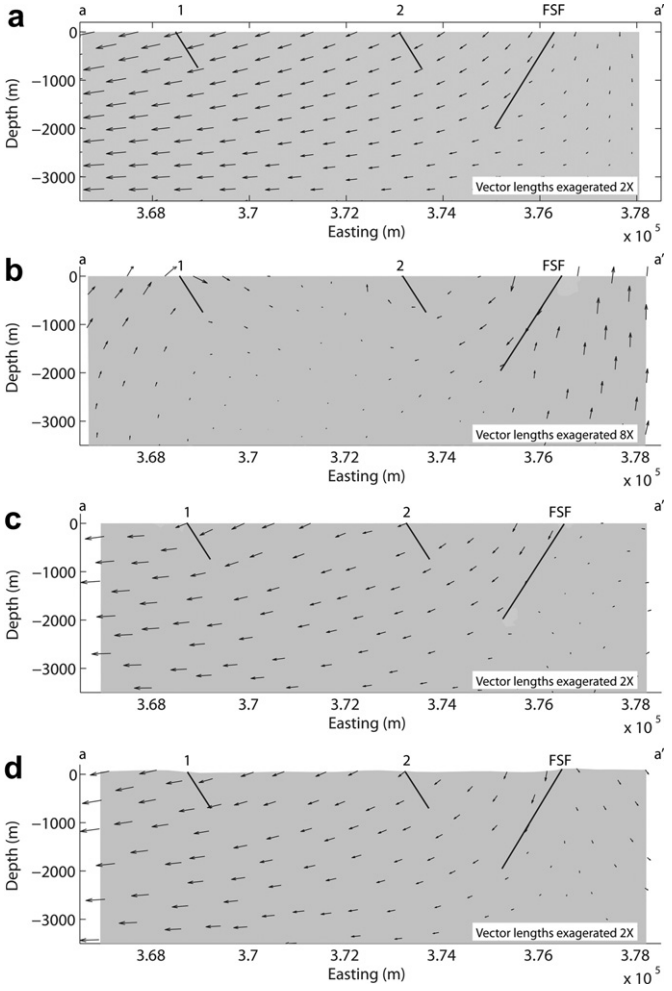

Fig. 7. In-plane displacement on cross-section a–a' (Fig. 3) as calculated by a) forward model in Poly3D, b) restoration boundary conditions alone, c) restoration boundary conditions supplemented by reverse tectonic boundary conditions, and d) reverse tectonic boundary conditions alone. Displacement is referenced to zero at 4 km depth, on the eastern edge of the cross-section. All displacement vectors are exaggerated by a factor of two, except (b), which is exaggerated by a factor of eight.

5.1. Retrodeformational models with restoration BCs only

Similar to the synthetic example discussed previously, the restoration model representing the Volcanic Tableland, in which all boundaries, except the horizon to be restored, are treated as traction-free (Figs. 5b, 6b, 7b), results in strain and displacement fields that bear little semblance to the kinematic behavior that might be expected from forward deformation (Figs. 5a, 6a, 7a). The marked contrast of both magnitude and orientation of ε_1 (Fig. 5a and b) and the differences in displacement vector fields (Fig. 7a and b) highlight the implications of failing to reverse the tectonic loads. Similar to the synthetic examples discussed previously, this model fails to capture the far-field extension that produced the Tableland fault array.

Vertical strain distributions emphasize the effects of the unphysical restoration BC particularly well. The forward model (Fig. 6a) suggests relatively uniform vertical contraction with magnitude generally somewhat less than 1%. Despite zero vertical stress, vertical contraction follows from far-field horizontal extension, due to Poisson's effect. The restoration model (Fig. 6b) differs in two obvious ways. First, average vertical strain is more nearly zero because of the absence of reverse tectonic boundary conditions. Second, large vertical strain perturbations (both positive and negative) are pervasive in the near surface. These perturbations result from tractions associated with displacements prescribed on the earth's surface. The largest perturbations are found near fault scarps, but others are isolated from modeled faults.

5.2. Retrodeformational models with restoration BCs supplemented by reverse tectonic loads

When considering restoration boundary conditions supplemented by reverse tectonic loads, the principal of superposition enables us to consider the loads applied in any order. It is constructive to consider the reverse tectonic load applied first. This restores, without violating the traction-free surface, what topography it may, and then the restoration boundary condition restores the rest. Although these models result in kinematics (Figs. 5c, 6c, 7c) that match forward models better than models with restoration boundary conditions alone, the question persists whether deformation due to restoration BCs is meaningful. Because vertical displacement boundary conditions on the earth's surface are unphysical and the structures that cause topography may be either improperly represented or entirely absent from the model, strain

Table 1
Results of forward and retrodeformational models of the Volcanic Tableland as seen on cross-section a–a'. Italicized text indicates critical differences between forward and retrodeformational models.

Model type:	Maximum principal strain (ε_1)	Vertical strain (ε_{zz})	Displacement vector field
Forward (Poly3D)	Fig. 5a • Generally sub-horizontal. • Uniform magnitude (~2%) distal from faults. • Magnitude reduced near fault surfaces and near FSF ε_1 is oriented parallel to fault (perpendicular to section) • Extensional and contractional quadrants observed near fault tips, as expected in linear elastic model.	Fig. 6a • Generally homogeneous, ~1%. • Reduced magnitude near fault surfaces • Well defined positive and negative quadrants in vicinity of fault tips.	Fig. 7a • With lower right corner fixed, vertical displacement component increases upward and horizontal displacement increases to the left. • Discrete discontinuity apparent across FSF but less apparent across smaller faults.
Restoration BCs only; vertical model boundaries traction-free	Fig. 5b • *Orientations highly heterogeneous.* • *Magnitude near zero throughout much of model space.* • *Several regions of localized but intense extension occur near earth's surface in footwall of faults and are characterized by near vertical ε_1.* • *Extensional and contractional quadrants near fault tips are not clearly evident.*	Fig. 6b • *Near zero magnitude distal from earth's surface and fault surfaces.* • *Heterogeneous, with large positive and negative perturbations pervasive near earth's surface. The largest perturbations coincide with fault scarps, but perturbations also occur elsewhere.*	Fig. 7b • *Heterogeneous, non-systematic orientation.* • *Displacement vectors are predominantly vertical.* • *Magnitudes consistently less than forward models.*
Restoration BCs and reverse tectonic (paleostress) BCs	Fig. 5c • Average strain magnitude ~2%. • Orientation sub-horizontal throughout most model space. • Extensional fault tip related perturbations are observed only for Fault 1 and FSF; *contractional perturbations entirely absent.* • *Large positive perturbations near earth's surface in footwall of FSF and Fault 1.* • *Short vectors at model center indicate significant out-of-plane rotation of ε_1.*	Fig. 6c • Magnitude ~1% distal from earth's surface and fault surfaces. • *Heterogeneous, with large positive and negative perturbations pervasive near earth's surface. The largest perturbations coincide with fault scarps, but perturbations also occur elsewhere.*	Fig. 7c • With lower right corner fixed, vertical displacement component increases upward and horizontal displacement increases to the left. • Discrete discontinuity apparent across FSF but less apparent across smaller faults.
Reverse tectonic (paleostress) BCs only; no restoration BC	Fig. 5d • Average strain magnitude ~2% • Orientation sub-horizontal throughout most model space. • *ε_1 rotated north–south near earth's surface in footwall of FSF.* • *Quadrants of extension and contraction around fault tips are generally less well defined than in forward model (except FSF extensional perturbation).*	Fig. 6d • Generally homogeneous, ~1%. • *Slightly greater heterogeneity than forward model.* • Reduced magnitude near fault surfaces. • Broadly defined positive and negative quadrants in vicinity of fault tips.	Fig. 7d • With lower right corner fixed, vertical displacement component increases upward and horizontal displacement increases to the left. • Discrete discontinuity apparent across FSF but less apparent across smaller faults.

patterns and displacement fields produced by the restoration boundary condition provide little, if any, geological insight.

The magnitude and orientation of strain fields calculated from forward models and from restoration models supplemented by reverse tectonic boundary conditions are similar in much of the cross-section, but there are locally significant differences. The models differ most in the near surface. Large strain perturbations are a direct result of the unphysical restoration boundary condition that violates the traction-free nature of the earth's surface. Thus, they appear most strongly in the vertical component of strain, parallel to the driving force, and tend to fade in magnitude radially, away from a focal point at the surface. Perturbations represent topography (and, presumably, some form of geologic strain) that is not flattened by the reverse BCs, perhaps because of inelastic processes, or association with structures that are inappropriately represented or absent from the simplified model. However the strain perturbations resulting from restoration boundary conditions do not indicate the nature or orientation of the geologic structure that produced the topographic feature and, in fact, some topography may not be structural in origin.

Positive vertical strain perturbations, as are evident in Fig. 6c, might suggest horizontal opening-mode fractures, for which field evidence is lacking in the Tableland. We know from field observations that much of this topography that is not restored by reverse boundary conditions and that, when restored, generates unphysical strain perturbations, is associated with smaller normal faults that are omitted from the simplified seismic-scale fault configuration. Given seismic data in which we could not see these smaller faults, we might infer the same conclusion that small topographic features are associated with small normal faults. However, the diffuse nature of restoration strain perturbations bears no resemblance to fault-related strain perturbations, and therefore should not be used to predict either fault geometry (perturbations for east or west-dipping faults are difficult to differentiate) or the potential extent or characteristics of fault-related damage. A critical examination of topography of the surface to be restored, in the context of the regional tectonic setting, provides as much, if not more, information than may be gleaned from analyzing strain in restoration models.

5.3. Retrodeformational models with reverse tectonic loads only

Kinematics of the pure reverse model (Figs. 5d, 6d, 7d) is quite similar to the forward model. This result is expected, given that elastic models with frictionless faults are reversible, the two models have the same fault configuration, and the boundary

conditions of the reverse model very nearly invert those of the forward model despite subtle differences in application of boundary conditions in finite element and boundary element methods. Neither forward nor reverse models are susceptible to the limitations of restoration boundary conditions.

Forward and reverse models each have benefits and drawbacks. In the case of the elastic models of the Tablelands, forward models provide improved resolution through the boundary element method. Reverse models do not capture the strain distributions around fault tips as well as forward models, in part because the coarse mesh discretization required for finite element simulations is unable to capture features smaller than the element dimension.

Reverse models offer the benefit of incorporating present day topography of the deformed horizon – the top of the Bishop Tuff in the Tableland case. Thus, by exporting the topography after retrodeformation (Fig. 8), it is possible to observe what topography can and cannot be explained by elastic deformation and slip on those faults represented in the model. If topographic heterogeneity is measured as the root mean square of vertical nodal coordinates after rotating and translating the surface such that the best-fitting plane is horizontal and passes through the origin, reverse boundary conditions reduce heterogeneity from 31.8 m to 28.3 m. Only 11% of topography is restored. The reverse tectonic loads back-slip those faults explicitly represented in the model, but all other topography remains. Including smaller Tableland faults in the model would likely account for some of the residual topography, but the small trace length and slip magnitude of most such faults suggests that their influence would be minimal. Attempts to evaluate a model including several of the next largest faults were abandoned due to mesh generation challenges. Perhaps retrodeformed topography could be used to help identify important structures that are absent from the model or to identify regions where the shortcomings of elasticity are most evident, though smoothing of topography in the coarse FEM mesh may limit such prospects.

In any real geologic situation, homogeneous far-field boundary conditions are unlikely to be capable of perfectly undoing observed deformation because of their idealized nature, the inherent nonlinearity of rock deformation, and because models of present day configuration are greatly simplified representations of geology. The systematic change in fault strike from NNE at the southern edge of the Tableland to NNW in the north (see Fig. 3) suggests that, in fact, principal stress and strain orientations may not be homogeneous throughout the Tableland; however, we assume homogeneous far-field stress and strain for the sake of model simplicity. A significant component of Tableland topography has likely been produced by smaller faults not included in our model, and much is undoubtedly associated with processes absent from the model and perhaps nonstructural in nature. That the reverse model restores only 11% of topography demonstrates the limitations of reverse elastic models and motivates the imposition of restoration boundary conditions. However, we must still ask what we might learn from forcing this topography to flatten, and if we might be better off working to generate an improved forward or reverse model.

5.4. Model strain as a predictor of subseismic faulting

A more practical evaluation of the application of retrodeformational models for prediction of strain and subseismic structures might be obtained directly from comparison of model strain with a map of all Tableland faults (Fig. 9). However, this comparison should be undertaken only with the recognition that small faults on the Tableland likely did not develop in response to stress/strain concentrations due to slip on larger faults, but rather large faults developed through coalescence of smaller faults (Dawers and Anders, 1995; Ferrill et al., 1999). Remaining small faults appear to be old faults that never coalesced, and today their growth is in fact inhibited – not enhanced – by the stress shadows of larger faults Lovely (2011).

Further, the models considered in this study, both forward and retrodeformational, do not account for the growth of faults. Geologically, not all faults originate at the same time, nor do faults originate instantaneously at their present size. By prescribing fault geometry based on present day fault dimensions, the models in this study are unable to account fully for the evolution of stress and strain fields as the Tableland fault system evolved. In the context of retrodeformational models, accounting for fault growth would require accurate knowledge of the relative ages of faults and their geometric growth, such that faults could be shrunk and sequentially removed during the simulation. We do not consider fault evolution for the sake of simplicity—age relations are not readily available and the sequence of fault evolution is beside the focus of this manuscript.

Nonetheless, comparison of model strain with detailed fault maps provides several interesting insights. Having demonstrated the clear benefits of supplementing restoration BCs with appropriate

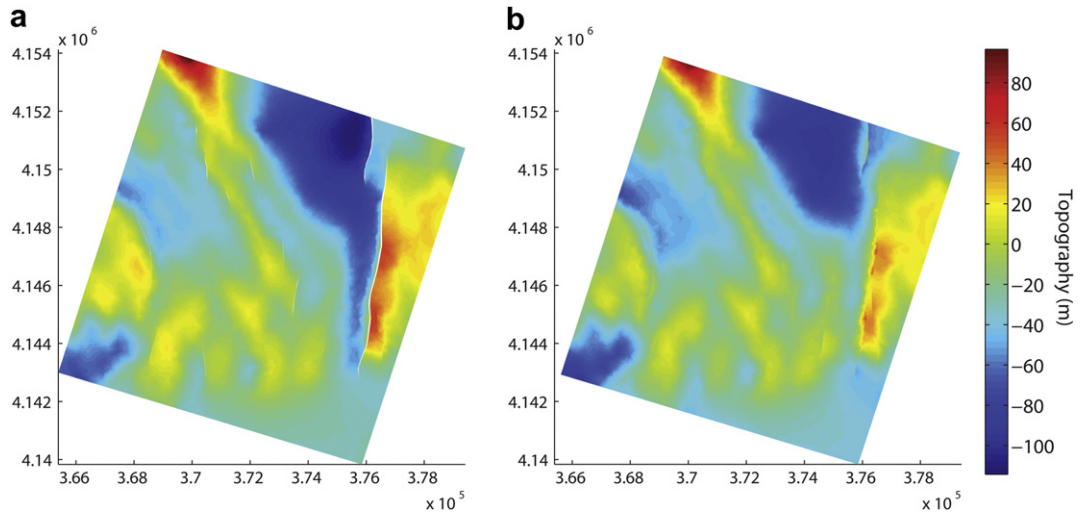

Fig. 8. Topography of the FEM model's surface in a) undeformed (present day) state and b) deformed by reverse tectonic boundary conditions.

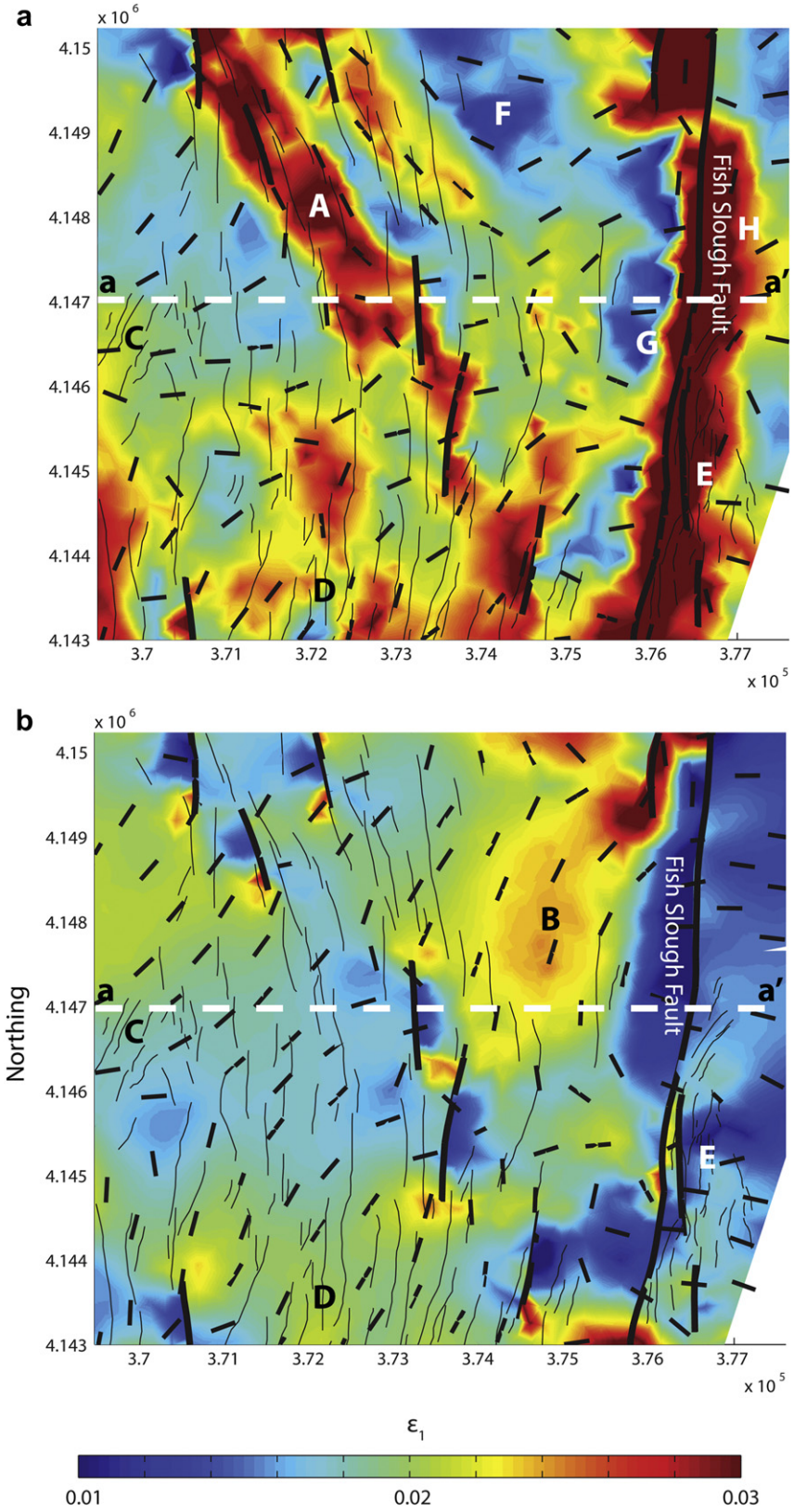

Fig. 9. Maps of maximum principal strain (ε_1) magnitude for a) restoration model with reverse tectonic boundary conditions and b) FEM model with reverse tectonic loads only. Results from models corresponding to cross-section views presented in Fig. 5c and d, respectively. Bold lines represent faults included in models as sliding contact surfaces and thin lines represent other faults mapped in the field. Short, intermediate weight lines represent intermediate principal strain orientation, which is the expected strike of small faults or joints if strain is an appropriate predictor of small structures. The white dashed line a–a' represents the location of cross-sections presented in Figs. 5–7.

reverse tectonic BCs, we compare smaller faults mapped in the field with maximum principal strain at the earth's surface from this model (Fig. 9a) and from the reverse tectonic model, in which restoration BCs do not violate the earth's traction-free surface (Fig. 9b). Black vectors represent the local orientation of ε_2. If model strain were an accurate predictor of subseismic-scale faulting, we would expect subseismic-scale faulting to be densest where extensional strain is greatest, and we might expect that normal faults would strike parallel to ε_2. Given the limitations of restoration boundary conditions, it is not altogether surprising to find that the correlation of restoration strain magnitude and orientation with subseismic-scale faulting is weak at best (Fig. 9a); the correlation with strain from the reverse tectonic model (Fig. 9b) is similarly limited.

Regions of maximum extension in Fig. 9a occur in the vicinity of point A and around Fish Slough fault (e.g. points E and H). The only one of these areas that corresponds to a large density of faults is around point E, in the footwall of the southern half of Fish Slough fault. There are no subseismic faults observed near the northern portion of Fish Slough fault, where the strain concentration is equally large, and around point A subseismic fault density is average, but not unusually large. However, there is a system of relatively large echelon faults running through this corridor, which were studied by Dawers and Anders (1995). The flattening of topography associated with these scarps is the source of strain in the restoration model. Some, though not all, of these faults are large enough to be represented in the seismic-scale fault model. Thus, a relatively large amount of strain may be accommodated by the faults in this region. However, the discrete fault scarps responsible for the distributed zone of strain may be easily identified in the 1/3 arc-second DEM, and the restoration model provides little or no additional geologic insight than could be extracted by careful analysis of raw topography.

Subseismic fault density is greatest around points C and D (Fig. 9a), where large extensional strain concentrations do not appear in the restoration results. Low fault density predictions would be appropriate near points F and G, where a significant strain shadow is observed in the vicinity of Fish Slough. However, there are a few faults in these vicinities, and the predicted orientation would be erroneous. In the vicinity of points C, F, and E, we might predict east-west striking faults, rather than the north–south striking faults that are observed across the Tableland. The limited nature of the correlations between restoration strain and subseismic fault density, and between strain orientation and fault orientation provide direct field evidence to supplement our theoretical argument why restoration strain should not be used to predict subseismic-scale structures.

Similar to cross-sections (Figs. 5–7), strain distributions suggested by the reverse tectonic model (Fig. 9b) are very different from those suggested by the restoration model (Fig. 9a). Interestingly, this model suggests opposite results of the restoration model in some areas where the restoration model correlates well with subseismic fault density; however, such results might be expected, since small faults do not necessarily form in response to strain concentrations associated with slip on larger faults. For example, there is a strain shadow, rather than concentration, around Fish Slough fault, including in the vicinity of point E, where subseismic faulting is intense. In the vicinity of point B, where no subseismic faults are observed, we see a positive strain perturbation (faulting would be expected here), whereas we see negative perturbations around point F in the model with restoration boundary conditions. The reverse model, despite being more mechanically sound, does no better predicting subseismic-scale faulting than does the restoration model. It might do a bit better regarding fault strike, although it predicts east-west striking faults around point C and east of Fish Slough fault, but the correlation between subseismic fault density and ε_1 magnitude is, in fact, probably worse.

6. Summary

The future of restoration, whether mechanics-based or not, seems limited to first-order kinematic analysis. Many of the touted benefits of mechanics-based restoration are real, including conservation of mass and momentum and the ability to simulate mechanical interaction of fault segments, heterogeneous slip distributions in three dimensions, out-of-plane strain and displacement, and strike-slip on faults. In complicated three-dimensional systems, mechanics-based restoration provides distinct benefits over kinematic methods for validation of structural interpretation (e.g. verifying that back-slipping a fault on a young horizon results in appropriate back-slip on the same fault in the context of older, deeper horizons), for reconstructing initial (undeformed) configuration of complicated faulted and folded systems, and for visualizing the 3D evolution of such structures. However, strain fields and subtle features of displacement fields from mechanics-based restoration, even when supplemented by appropriate reverse tectonic boundary conditions, should be treated with skepticism. The perturbations observed in restoration models of the Tableland are unlikely to result from mechanically valid tectonic processes. Mechanics-based restoration models, because of their unphysical boundary conditions, should not be treated as equivalent to forward mechanical models.

Perhaps the greatest advantage to forward models is that they allow one to incorporate non-linear elasto-plastic and visco-plastic constitutive laws, which are more appropriate for rock deformation over geologic time, and frictional sliding on fault surfaces. Such models may account for the effects of compaction and pore pressure using principles of mechanics in coupled poro-mechanical simulations. Increasingly sophisticated numerical models, if applied appropriately, will allow structural geologists in the future to simulate kinematics with increasing accuracy and to better predict not only regions of localized strain, but also in-situ stress distributions throughout geologic history. Because entropy is a one way street, and because non-linear constitutive laws are highly sensitive to load path and therefore do not behave in the same way for forward deformation and retrodeformation, forward mechanical models are the only way to capture the true nature of rock deformation without employing non-linear inversion techniques that would require currently unavailable computational power.

Increasingly sophisticated forward models, whose construction (e.g. initial geometric configuration) might be guided by the kinematic behavior of retrodeformational models, are the most appropriate way to simulate geologic deformation and to predict stress, strain, and associated small-scale features. Nonetheless, we acknowledge that in some tectonic settings, the Tableland being a prime example, where there is not a causative link from large to smaller structures, it is never appropriate to predict smaller structures from strain (or stress) due to slip on larger faults.

7. Conclusions

Mechanics-based restoration methods provide significant improvement over traditional kinematic methods – improvements that have been touted as providing a means to predicting geologic strain and displacement fields from numerical models that do not require assumptions about the initial state of the deformational system, but rather begin with the present day, observed geometric configuration and work backwards. Despite the reversible nature of

the assumed (albeit simplified) linear elastic constitutive law, restoration boundary conditions are mechanically inappropriate. They violate the traction-free nature of the earth's surface, and restoration models as performed to date do not account for tectonic loads that are presumed as the driving mechanism behind forward deformation.

Synthetic examples and analysis of field data from the Volcanic Tableland extensional fault system demonstrate that the potential implications of boundary conditions must be carefully considered before interpreting geologic deformation from mechanics-based restoration models. We suggest that mechanics-based restoration models are a valid tool for verification of structural interpretation and for first-order illustration of the kinematic evolution of a 3D structure, but even when supplemented with appropriate reverse tectonic boundary conditions, restoration models may not accurately predict geologic strain and should not be used to infer small-scale structures that might be associated with such perturbations. We suggest that elastic reverse models governed only by physically appropriate reverse tectonic boundary conditions may be used to extract geologic strain and displacement, although one must be cognizant that elasticity is a dramatic simplification of the complicated constitutive laws that govern rock deformation on a geologic time scale.

The kinematics suggested by reverse models are nearly identical to the kinematics of forward elastic models, and enable visualization of the retrodeformed topography and comparison with the present day topography in order to understand what may and what may not be accounted for by the simplified elastic model. Forward models, however, are clearly the best route forward to predict geologic deformation in the subsurface because, in addition to physically plausible boundary conditions that simulate tectonic loads and do not violate the earth's traction-free surface, they may account for inelastic deformation and other non-linear material behaviors that characterize rock deformation over geologic time scales. Although retrodeformational models may capture strain and displacement fields with variable degrees of accuracy, well designed forward models with appropriate material properties should provide increasingly accurate kinematic results and such models are the only way to simulate geologically appropriate stress distributions.

Acknowledgements

The authors wish to thank Igoess – a Schlumberger Company, for providing software and support for Dynel3D and Poly3D, and the Chevron Corporation for permission to publish this manuscript. Bishop Tablelands LiDAR data provided courtesy of Chevron Corporation. Constructive reviews from Peter Huddleston and Delphine Rouby, editorial comments from Richard Groshong, and discussion with George Hilley provided valuable feedback that improved this manuscript significantly.

Appendix A. Paleostress analysis using mechanics

Unlike the well known method of paleostress analysis that is based on the Wallace–Bott hypothesis (Wallace, 1951; Bott, 1959; Ramsay and Lisle, 2000), mechanics-based paleostress analysis implements a least squares inversion to calculate the components of the far-field stress tensor that best reproduce observed slip on faults modeled in an elastic continuum. Thus, it provides a means of defining idealized tectonic boundary conditions for forward and reverse elastic models that most accurately reproduce fault slip everywhere that slip measurements may be made. We use a code developed by IGEOSS, which is based on the forward problem solved by Poly3D (Thomas, 1993). Faults are discretized as triangular elements of constant displacement discontinuity implemented in a linear elastic half-space. In Poly3D, far-field stress may be prescribed, and slip is calculated such that the shear traction resolved on each triangular element is relaxed completely. The paleostress inversion calculates the three horizontal components of the far-field stress (σ_{xx}, σ_{yy} and σ_{xy}; vertical components $\sigma_{xz} = \sigma_{yz} = \sigma_{zz} = 0$ are prescribed) in order to minimize the difference between observed slip and model slip on all elements where slip is known. Prescribing the vertical component of the stress tensor as zero is justified because continuum deformation is elastic and faults are frictionless; therefore, only the deviatoric component of the stress tensor influences fault slip and it is unnecessary to account for the lithostatic stress gradient. It is generally accepted that a principal stress is vertical because the earth's surface is traction-free (e.g. Lisle et al., 2006; Zoback, 2007). The paleostress inversion implementation is described in detail by Kaven (2009) and Maerten (2010).

The paleostress tensor for the Volcanic Tableland is calculated using the seismic-scale fault model described previously. Dip-slip is derived from profiles of throw across fault scarps, which are extracted from a digital elevation model (DEM) with 2 m resolution generated from airborne laser swath mapping (ALSM, also known as airborne LiDAR) data (Fig. 3). The ALSM survey was acquired by Chevron through a commercial vendor. ALSM methods are capable of mapping topography with decimeter vertical precision (Shrestha et al., 1999). Dip-slip constraint is prescribed for the paleostress inversion on all fault surface elements that intersect the earth's surface within the coverage area of the ALSM data, although the fault model extends beyond the ALSM data to the north and west, and all faults are allowed to slip in order to account for their interaction in a more complete mechanical system. Strike-slip is constrained to zero on these same elements in light of field evidence that strike-slip is insignificant (Bateman et al., 1965; Dawers et al., 1993; Dawers and Anders, 1995).

Initial paleostress calculations suggested tensile stress in excess of 100 MPa and oriented north–south, parallel to the average fault strike. Such an unphysical result (most tensile stress should be perpendicular to fault strike in a normal fault regime (Anderson, 1951)) is the result of an ill-conditioned inverse problem (e.g. Aster et al., 2005) in which all fault elements are nearly parallel to each other. Because the north–south (fault-parallel) component of the stress tensor resolves little traction on fault surface elements, it has little effect on fault slip, and this component of the paleostress tensor is essentially unconstrained.

Maerten (2010) introduces a Monte-Carlo approach to solving the paleostress problem which may incorporate additional data types, including fault and fracture orientation and displacement fields (e.g. GPS, InSAR), which could help to overcome the ill-conditioning of this initial model. However, we address ill-conditioning by including one additional fault in the paleostress inversion (Fig. 3). This fault, located in the southwest corner of the Tableland, is unusual because it strikes northeast-southwest, and therefore the north–south component of the stress tensor resolves significant traction on its surface. The fault is relatively large, with throw locally exceeding 20 m, although not consistently. It alone is added to the set of faults used for paleostress inversion, although there are about five other faults of comparable size that are omitted. Because this fault is beyond the extent of the ALSM data, throw is mapped from the coarser and less precise National Elevation Dataset 1/3 arc-second DEM (Maune, 2007), the same DEM used to represent topography in FEM models. The improved paleostress tensor suggests maximum tension oriented N72°W, with a magnitude of 62 MPa, and an intermediate principal stress of 51 MPa oriented N18°E. Root mean square residuals are relatively large, 19.6 m for dip-slip and 7.5 m for strike-slip.

Although paleostress magnitudes do not account for lithostatic stress gradient, suggested stresses are nearly an order of magnitude greater than the tensile strength of rock, which is generally about 10 MPa (Bieniawski, 1984). Considering our choice of a minimal elastic stiffness (2.5 GPa, *Geologic model* section), it is clear that inelastic deformation must play a significant role in Tableland deformation. One might argue that even forward and reverse BCs are, in this sense, unphysical; however, by Hooke's law the paleostress tensor equates to far-field strains of 2.0% and 1.4%, oriented N72°W and N18°E, respectively. Such strain magnitudes are physically realistic and comparable to geologic estimates of strain accommodated across the Tableland (e.g. Pinter, 1995), and produce fault-related deformation patterns similar to inelastic models Lovely (2011).

Results of the paleostress analysis are not necessarily intuitive. Minimum horizontal extension is unexpectedly large and the N72°W orientation of maximum tension/extension, while perhaps in accord with strike-slip observed on basin-bounding faults, is unexpected from an optimization that minimizes strike-slip on Tableland faults that strike, on average, north–south (Fig. 3). The unexpectedly large magnitude of minimum horizontal extension may be attributed to heterogeneous fault orientation; horizontal stress components of comparable magnitude minimize strike-slip on faults of any orientation by minimizing shear stress in the horizontal plane. Further, the relatively similar magnitude of principal stresses in the horizontal plane minimizes sensitivity of the inversion to principal stress orientation. However, clockwise rotation of the optimized stress tensor may be attributed to the requirement that strike-slip be minimized on all modeled faults, including the NE–SW striking fault and FSF, which strikes NNE and, being the largest fault in the model, has a disproportionate influence on the inversion. The systematic change in fault strike from NNE at the southern edge of the Tableland to NNW in the north (see Fig. 3) suggests that, in fact, principal stress and strain orientations may not be homogeneous throughout the Tableland. However, we assume homogeneous far-field stress and strain for the sake of model simplicity and accept the limitations of paleostress inversion because potential shortcomings do not negate conclusions of this study as they pertain to restoration results.

References

Allmendinger, R.W., Figueroa, D., Snyder, D., Beer, J., Mpodozis, C., Isacks, B.L., 1990. Foreland Shortening and Crustal balancing in the Andes at 30°S Latitude. Tectonics 9 (4), 789–809.

Anderson, E.M., 1951. The Dynamics of Faulting. Oliver and Boyd, Edinburgh, 206 p.

Aster, R.C., Thurber, C.H., Borchers, B., 2005. Parameter Estimation and Inverse Problems. Elsevier Academic Press, Amsterdam, 301 p.

Avar, B.B., Hudyma, N., Karakouzian, M., 2003. Porosity dependence of the elastic modulus of lithophysae-rich tuff: numerical and experimental investigations. International Journal of Rock Mechanics and Mining Sciences 40 (6), 919–928.

Aydin, A., Schultz, R.A., 1990. Effect of mechanical interaction on the development of strike-slip faults with echelon patterns. Journal of Structural Geology 12 (1), 123–129.

Aydin, A., Borja, R.I., Eichhubl, P., 2006. Geological and mathematical framework for failure modes in granular rock. Journal of Structural Geology 28 (1), 83–98.

Bailey, R.A., Dalrymple, G.B., Lanphere, M.A., 1976. Volcanism, structure, and geochronology of long Valley Caldera, Mono County, California. Journal of Geophysical Research 81 (5), 725–744.

Bally, W.W., Gordy, P.L., Stewart, G.A., 1966. Structure, seismic data, and orogenic evolution of southern Canadian Rocky Mountains. Bulletin of Canadian Petroleum Geology 14, 337–381.

Bateman, P.C., Pakiser, L.C., Kane, M.F., California-Division of Mines and Geology, 1965. Geology and Tungsten Mineralization of the Bishop District, California. U.S. Govt. Print. Off., Washington, 208 p.

Benesh, N.P., Plesch, A., Shaw, J.H., Frost, E.K., 2007. Investigation of growth fault bend folding using discrete element modeling: implications for signatures of active folding above blind thrust faults. Journal of Geophysical Research-Solid Earth 112.

Bieniawski, Z.T., 1984. Rock Mechanics Design in Mining and Tunneling. A.A. Balkema, Rotterdam, 272 p.

Bott, M.H.P., 1959. The mechanics of oblique slip faulting. Geology Magazine 96, 109–117.

Boyer, S.E., Elliott, D., 1980. Thrust systems. AAPG Bulletin 66 (9), 1196–1230.

Burgmann, R., Pollard, D.D., Martel, S.J., 1994. Slip distributions on faults: effects of stress gradients, inelastic deformation, heterogeneous host-rock stiffness, and fault interaction. Journal of Structural Geology 16 (12), 1675–1690.

Byerlee, J., 1978. Friction of rocks. Pure and Applied Geophysics 116, 615–626.

Carey, W.S., 1962. Folding. Journal of Alberta Petroleum Geology 10, 95–144.

Chamberlain, R.T., 1910. Appalachian folds of Central Pennsylvania. The Journal of Geology 18 (3), 228–251.

Chou, P.C., Pagano, N.J., 1967. Elasticity; Tensor, Dyadic, and Engineering Approaches. Van Nostrand, Princeton, N.J., 290 p.

Cooke, M.L., Marshall, S.T., 2006. Fault slip rates from three-dimensional models of the Los Angeles metropolitan area, California. Geophysical Research Letters 33 (21).

Dahlstrom, C.D.A., 1969. Ballanced cross section. Canadian Journal of Earth Sciences 6, 743–757.

Dawers, N.H., Anders, M.H., 1995. Displacement-Length scaling and fault Linkage. Journal of Structural Geology 17 (5), 607–614.

Dawers, N.H., Anders, M.H., Scholz, C.H., 1993. Growth of normal faults - Displacement-length scaling. Geology 21 (12), 1107–1110.

Dinwiddie, C.L., Bradbury, K.K., McGinnis, R.N., Fedors, R.W., Ferrill, D.A., 2006. Fault zone deformation overprints permeability of nonwelded ignimbrite: Chalk cove fault, Bishop Tuff, Bishop, California. Vadose Zone Journal 5 (2), 610–627.

Dula, W.F., 1991. Geometric-Models of Listric normal faults and Rollover folds. AAPG Bulletin 75 (10), 1609–1625.

Erickson, S.G., Jamison, W.R., 1995. Viscous-Plastic finite-element models of fault-bend folds. Journal of Structural Geology 17 (4), 561–573.

Erslev, E.A., 1991. Trishear fault-propagation folding. Geology 19 (6), 617–620.

Evans, J.P., Bradbury, K.K., 2004. Faulting and fracturing of nonwelded Bishop Tuff, eastern California: deformation mechanisms in very porous materials in the vadose zone. Vadose Zone Journal 3 (2), 602–623.

Ferrill, D.A., Morris, A.P., 2001. Displacement gradient and deformation in normal fault systems. Journal of Structural Geology 23 (4), 619–638.

Ferrill, D.A., Stamatakos, J.R., Sims, D., 1999. Normal fault corrugation: implications for growth and seismicity of active normal faults. Journal of Structural Geology 21, 1027–1038.

Ferrill, D.A., Morris, A.P., Stamatakos, J.A., Sims, D.W., 2000. Crossing conjugate normal faults. AAPG Bulletin 84 (10), 1543–1559.

Fletcher, R.C., Pollard, D.D., 1999. Can we understand structural and tectonic processes and their products without appeal to a complete mechanics? Journal of Structural Geology 21, 1071–1088.

Gibbs, A.D., 1983. Balanced cross-section construction from seismic sections in areas of extensional tectonics. Journal of Structural Geology 5 (2), 153–160.

Gilbert, C.M., 1938. Welded tuff in eastern California. Geological Society of America Bulletin 49, 1829–1861.

Goethals, M.M., Niedermann, S., Hetzel, R., Fenton, C.R., 2009. Determining the impact of faulting on the rate of erosion in a low-relief landscape: a case study using in situ produced ^{21}Ne on active normal faults in the Bishop Tuff, California. Geomorphology 103, 401–413.

Griffiths, P., Jones, S., Salter, N., Schaefer, F., Osfield, R., Reiser, H., 2002. A new technique for 3-D flexural-slip restoration. Journal of Structural Geology 24 (4), 773–782.

Griggs, R.F., 1922. The Valley of Ten Thousand Smokes. National Geographic Society, Washington, 341 p.

Guzofski, C.A., Mueller, J.P., Shaw, J.H., Muron, P., Medwedeff, D.A., Bilotti, F., Rivero, C., 2009. Insights into the mechanisms of fault-related folding provided by volumetric structural restorations using spatially varying mechanical constraints. AAPG Bulletin 93 (4), 479–502.

Hardy, S., Ford, M., 1997. Numerical modeling of trishear fault propagation folding. Tectonics 16 (5), 841–854.

Hardy, S., Finch, E., 2005. Discrete-element modeling of detachment folding. Basin Research 17, 507–520.

Hollett, K.J., Inyo County (Calif.), Los Angeles (Calif.). Dept. of Water and Power, 1991. Geology and Water Resources of Owens Valley, California. United States Government Printing Office, Washington, 77 p.

Hunt, C.W., 1957. Planimetric equation. Journal of Alberta Petroleum Geology 5, 229–241.

Izett, G.A., Obradovich, J.D., 1994. Ar-40/Ar-39 age constraints for the Jaramillo normal Subchron and the Matuyama-Brunhes Geomagnetic boundary. Journal of Geophysical Research-Solid Earth 99 (B2), 2925–2934.

Jaeger, J.C., Cook, N.G.W., Zimmerman, R.W., 2007. Fundamentals of Rock Mechanics, fourth ed.. Blackwell Pub., Malden, MA, 475 p.

Kattenhorn, S.A., Pollard, D., 2001. Integrating 3-D seismic data, field analogs, and mechanical models in the analysis of segmented normal faults in the Wytch Farm oil field, southern England, United Kingdom. AAPG Bulletin 85 (7), 1183–1210.

Kaven, J.O., 2009. Geometry and Mechanics of Three-dimensional Faults: Implications for Slip, Aftershocks, and Paleostress. Stanford University, Stanford, 166 p.

Kirby, E., Burbank, D.W., Reheis, M., Phillips, F., 2006. Temporal variations in slip rate of the white Mountain fault zone, eastern California. Earth and Planetary Science Letters 248 (1–2), 168–185.

Lin, M., Brechtel, C.E., Hardy, M.P., Bauer, S.J., 1993. Rock mass mechanical property estimation strategy for the Yucca Mountain site characterization project, High Level Radioactive Waste Management. In: Proceedings of the Fourth Annual International Conference, vol. 1, pp. 937–942.

Lisle, R.J., Orife, T.O., Arlegui, L., Liesa, C., Srivastava, D.C., 2006. Favoured states of palaeostress in the Earth's crust: evidence from fault-slip data. Journal of Structural Geology 28 (6), 1051–1066.
Lovely, P., 2011. Fault-related Deformation over Geologic Time: Integrating Field Observations, High Resolution Geospatial Data and Numerical Modeling to Investigate 3D Geometry and Non-linear Material Behavior. 245 p., Stanford,CA.
Maerten, F., 2010. Geomechanics to Solve Geological Structure Issues: Forward, Inverse and Restoration Modeling. Universite Montpellier II, Montpellier. 455 p.
Maerten, F., Maerten, L., Cooke, M., 2009. Solving 3D boundary element problems using constrained iterative approach. Computational Geosciences 14 (4), 551–564.
Maerten, L., Maerten, F., 2006. Chronologic modeling of faulted and fractured reservoirs using geomechanically based restoration: technique and industry applications. AAPG Bulletin 90 (8), 1201–1226.
Maerten, L., Gillespie, P., Daniel, J.M., 2006. Three-dimensional geomechanical modeling for constraint of subseismic fault simulation. AAPG Bulletin 90 (9), 1337–1358.
Malvern, L.E., 1969. Introduction to the Mechanics of a Continuous Medium, vol. xii. Prentice-Hall, Englewood Cliffs, N.J. 713 p.
Manighetti, I., King, G.C.P., Gaudemer, Y., Scholz, C.H., Doubre, C., 2001. Slip accumulation and lateral propagation of active normal faults in Afar. Journal of Geophysical Research 166 (B7), 13667–13696.
Maune, D.F., 2007. Digital Elevation Model Technologies and Applications: The DEM Users Manual, second ed.. American Society for Photogrammetry and Remote Sensing, Bethesda, Md. 655 p.
Moretti, I., 2008. Working in complex areas: new restoration workflow based on quality control, 2D and 3D restorations. Marine and Petroleum Geology 25 (3), 205–218.
Moretti, I., Lepage, F., Guiton, M., 2006. KINE3D: a new 3D restoration method based on a mixed approach linking geometry and geomechanics. Oil and Gas Science and Technology 61 (2), 277–289.
Morgan, J.K., McGovern, P.J., 2005. Discrete element simulations of gravitational volcanic deformation: 1. Deformation structures and geometries. Journal of Geophysical Research-Solid Earth 110 (B5).
Muron, P., 2005. 3-D Numerical Methods for the Restoration of Faulted Geological Structures. Institut National Polytechnique de Lorraine, Lorraine. 141 p.
Pinter, N., 1995. Faulting on the volcanic Tableland, Owens Valley, California. Journal of Geology 103 (1), 73–83.
Plesch, A., Shaw, J.H., Kronman, D., 2007. Mechanics of low-relief detachment folding in the Bajiaochang field, Sichuan Basin, China. AAPG Bulletin 91 (11), 1559–1575.
Pollard, D.D., Aydin, A., 1988. Progress in understanding jointing over the past Century. Geological Society of America Bulletin 100 (8), 1181–1204.
Pollard, D.D., Fletcher, R.C., 2005. Fundamentals of Structural Geology. Cambridge University Press, Cambridge, UK. 500 p.
Ramsay, J.G., Huber, M.I., 1983. The Techniques of Modern Structural Geology. Academic Press, London/New York, 1–2 pp.
Ramsay, J.G., Lisle, R.J., 2000. The Fundamentals of Structural Geology. Academic Press, San Diego. 1061 p.
Rouby, D., Xiao, H., Suppe, J., 2000. 3-D restoration of Complexly folded and faulted surfaces using multiple unfolding mechanisms. AAPG Bulletin 84 (6), 805–829.
Rouby, D., Cobbold, P.R., Szatmarib, P., Demercianb, S., Coelhoc, D., Rici, J.A., 1993. Least-squares palinspastic restoration of regions of normal faulting—application to the Campos basin (Brazil). Tectonophysics 221 (3–4), 439–452.
Sanz, P.F., Borja, R.I., Pollard, D.D., 2007. Mechanical aspects of thrust faulting driven by far-field compression and their implications for fold geometry. Acta Geotechnica 2 (1), 17–31.
Sanz, P.F., Pollard, D.D., Allwardt, P.F., Borja, R.I., 2008. Mechanical models of fracture reactivation and slip on bedding surfaces during folding of the asymmetric anticline at Sheep Mountain, Wyoming. Journal of Structural Geology 30 (9), 1177–1191.
Schmalholz, S.M., 2008. 3D numerical modeling of forward folding and reverse unfolding of a viscous single layer: implications for the formation of folds and fold patterns. Tectonophysics 446, 31–41.
Segall, P., 2010. 432. Earthquake and Volcano Deformation, vol. xxiii. Princeton University Press, Princeton, N.J. p.
Shrestha, R.L., Carter, W.E., Lee, M., Finner, P., Sartori, M., 1999. Airborne laser swath mapping: accuracy assessment for surveying and mapping applications. Surveying and Land Information Systems 59 (2), 83–94.
Stockli, D.F., Dumitru, T.A., McWilliams, M.O., Farley, K.A., 2003. Cenozoic tectonic evolution of the White mountains, California and Nevada. Geological Society of America Bulletin 115 (7), 788–816.
Stockmal, G.S., Beaumont, C., Nguyen, M., Lee, B., 2007. Mechanics of thin-skinned fold-and-thrust belts: insights from numerical models. GSA Special Papers 433, 63–98.
Suppe, J., 1983. Geometry and kinematics of fault-bend folding. American Journal of Science 283, 684–721.
Thomas, A., 1993. Poly3D: A Three-dimensional Polygonal Element, Displacement Discontinuity Boundary Element Computer Program with Applications to Fractures, Faults, and Cavities in the Earth's Crust. Stanford University, Stanford. 221 p.
Wallace, R.E., 1951. Geometry of shearing stress and relation of faulting. Journal of Geology 59 (2), 118–130.
Wegner, J.L., Haddow, J.B., 2009. Elements of Continuum Mechanics and Thermodynamics. Cambridge University Press, Cambridge. 278 p.
White, N.J., Jackson, J.A., Mckenzie, D.P., 1986. The Relationship between the geometry of normal faults and that of the Sedimentary layers in their Hanging walls. Journal of Structural Geology 8 (8), 897–909.
Willemse, E.J.M., Pollard, D.D., Aydin, A., 1996. Three-dimensional analyses of slip distributions on normal fault arrays with consequences for fault scaling. Journal of Structural Geology 18 (2–3), 295–309.
Williams, G., Vann, I., 1987. The geometry of Listric normal faults and deformation in their Hanging walls. Journal of Structural Geology 9 (7), 789–795.
Wilson, C.J.N., Hildreth, W., 1997. The Bishop Tuff: new insights from eruptive stratigraphy. Journal of Geology 105 (4), 407–439.
Woodward, N.B., Boyer, S.E., Suppe, J., 1989. Balanced Geological Cross-sections: An Essential Technique in Geological Research and Exploration. American Geophysical Union, Washington, D.C. 132 p.
Yilmaz, Ö. g., Doherty, S.M., 2001. Seismic Data Analysis: Processing, Inversion, and Interpretation of Seismic Data, second ed.. Society of Exploration Geophysicists, Tulsa, OK. 2027 p.
Zoback, M.D., 2007. Reservoir Geomechanics. Cambridge University Press, Cambridge. 449 p.